

Chemical Vapor Deposition (CVD) Growth and Optimal Transfer Processes for Graphene

by
Seong Soon Jo

B.S., Materials Science and Engineering, Yonsei University, 2012
M.S., Materials Science and Engineering, Yonsei University, 2014

Submitted to the Department of Materials Science and Engineering
in partial fulfillment of the requirements for the degree of

Master of Science in Materials Science and Engineering

at the

MASSACHUSETTS INSTITUTE OF TECHNOLOGY

February 2018

© 2018 Massachusetts Institute of Technology. All rights reserved.

Signature of author _____
Department of Materials Science and Engineering
January 11, 2018

Certified by _____
Jing Kong
Professor of Electrical Engineering
Thesis Supervisor

Certified by _____
Caroline A. Ross
Associate Head, Department of Materials Science and Engineering
Thesis Supervisor

Accepted by _____
Donald R. Sadoway
John F. Elliott Professor in Materials Science and Engineering
Chair, Department Committee on Graduate Students

Chemical Vapor Deposition (CVD) Growth and Optimal Transfer Processes for Graphene

by

Seong Soon Jo

Submitted to the Department of Materials Science and Engineering
on January 19, 2018, in Partial Fulfillment of the
Requirements for the Degree of Master of Science in
Materials Science and Engineering

ABSTRACT

Graphene has been regarded as a good candidate to make a breakthrough in various applications including electronics, sensors and spintronics due to its exceptional physical properties. To realize those practical applications, a high quality homogeneous wafer-scale graphene is required. Among various synthesis methods, chemical vapor deposition (CVD) has been a focus of attention as the most promising and cost-efficient deposition techniques, with advantages of its excellent repeatability and controllability, to produce large area graphene crystals on transition metal catalyst substrates. In particular, Cu with low carbon solid solubility is suitable to obtain uniform single layer deposition of graphene over large areas. Here, we report reliable method to grow high-quality continuous graphene film by CVD. Their surface properties and electrical transport characteristics are explored by several characterization techniques. In CVD process, furthermore, a subsequent transfer process to a substrate of interest is required for a wide variety of applications, especially in electronics and photonics, because the metal substrates necessary to catalyze the CVD graphene growth cannot be used. It is important not only to improve quality of as-grown graphene by optimizing growth system but also to develop transfer methods to prevent degradation in quality while transferring as-grown graphene to target substrates. In the case of wet transfer, surface tension of the liquid such as an etching agent or water contributes to make inevitable ripples, wrinkles and cracks. In this regard, we demonstrate new transfer methods by selecting a new polymeric support materials in order to reduce the number of wrinkles, defects and residues.

Thesis Supervisor: Jing Kong

Title: Professor of Electrical Engineering

Acknowledgments

First, I would like to express my gratitude to my thesis advisor Jing Kong and co-advisor Caroline Ross. Especially, I really appreciate to Jing for giving me the support to do my work at MIT. This work would not have been possible without her thoughtful guidance.

I would also like to thank my family who have been very supportive and giving me eternal love. I especially need to thank my mother, Miyoung Park, and my father, Yiyeon Jo, for their guidance and insight.

I am grateful for all of my friends at MIT, who support me all the time. Thanks for making me smile.

Table of Contents

List of Figures

List of Tables

Chapter 1. Introduction	11
1.1. Background	11
1.2. Electronic structure of graphene and its properties	13
1.3. Graphene growth on transition metal substrates	14
1.4. Transfer process of CVD-grown graphene.....	16
1.5. Thesis objectives.....	17
Chapter 2. CVD growth of graphene.....	19
2.1. Synthesis of graphene on a Cu foil	19
2.1.1. Chemical pretreatment of Cu foil	19
2.1.2. Monolayer graphene by Low Pressure CVD (LPCVD)	21
2.1.3. Multilayer graphene by Ambient Pressure CVD (APCVD).....	22
2.2. Characterizations	23
2.2.1. Optical Microscopy (OM).....	23
2.2.2. Raman spectroscopy	24
2.2.3. Atomic Force Microscopy (AFM)	26
2.2.4. Scanning Electron Microscope (SEM)	28
2.2.5. Hall measurement	29
Chapter 3. Transfer process for graphene.....	30
3.1. Background	30
3.2. PMMA-mediated transfer.....	31
3.2.1. Limitation of the conventional transfer method.....	32
3.3. PDMS/PMMA double-layer transfer.....	33
3.3.1. Mechanism of the double-layer transfer method	34
3.3.2. Quantitative analysis of wrinkles in graphene	38

3.4. Wax-supported transfer	40
3.4.1. Mechanism of wax-mediated transfer method.....	42
3.4.2. Dependence of thermal expansion effect of wax on temperature.....	44
3.4.3. Improvement in surface quality	45
 Chapter 4. Conclusions	47
 References	48

List of Figures

Figure 1-1. Schematics of hexagonal crystal lattice and its corresponding Brillouin zone. (a) Honeycomb lattice structure of graphene with two atoms per unit cell, representing inequivalent carbon atoms A (blue) and B (yellow), the lattice unit vectors, \vec{a}_1 and \vec{a}_2 and the nearest-neighbor vectors, $\vec{\delta}_1$, $\vec{\delta}_2$, and $\vec{\delta}_3$. (b) Construction of first Brillouin zone of graphene, showing two distinct Dirac points K and K' , high symmetry points Γ , K , and M and the unit vectors in reciprocal space, \vec{b}_1 and \vec{b}_2 . (c) $E(k)$ dispersion curve of graphene for finite values of t and t' , with $t=2.7\text{eV}$ (the nearest-neighbor hopping energy) and $t' = -0.2t$ (the next nearest-neighbor hopping energy). Zoom in energy band structure close to one Dirac point (red circle).¹⁹ 14

Figure 1-2. Equilibrium phase diagram of (a) Ni-C binary system;²¹ (b) Cu-C binary system; (inset) zoom-in of Cu-C binary phase diagram at the Cu-rich region.²³ At 1000 °C, the carbon solubility (a) in Ni is ~ 1.1 at%, (b) in Cu is ~ 0.0006 at% 16

Figure 1-3. Surface roughness characterization, optical properties of graphene transferred by using different supporting materials. Graphene-based OLED. AFM images of (a) PMMA- and (b) rosin-mediated graphene. Small rosin residue particles are marked as the white circles. (c) a monolayer graphene film (blue dot square) with the size of 10 x10 cm² onto a polyethylene terephthalate (PET) film. (d) schematic of OLED device structure (left) and its energy band diagram (right). (e) plot of current intensity and luminance versus voltage respectively. (f) photo of large area flexible green OLED with a rosin-transferred five-layer graphene anode.²⁵ 18

Figure 2-1. Scanning Electron Microscope (SEM) images of a Cu foil with respect to different pre-cleaning methods. SEM images of the Cu surface chemically treated with (a)(c) acetic acid and (b)(d) nickel etchant in different magnification of (a)-(b) x500 and (c)-(d) x6000. 20

Figure 2-2. A schematic flow of single layer graphene growth by CVD system, illustrating the temperature profile as a function of time. 21

Figure 2-3. A schematic flow of multi-layer graphene growth by CVD system, representing the temperature profile as a function of time. 22

Figure 2-4. Optical Microscopy (OM) images of a CVD-grown graphene sheet on SiO₂/Si wafers. OM image of a monolayer graphene thin film (a) before the transition to continuous film. (b) a low magnification and (c) a high magnification OM images of homogenous and continuous film. (d) OM images of a few-layer graphene film. 24

Figure 2-5. Raman spectroscopy obtained from a CVD-grown graphene after transferred onto the SiO₂/Si wafer. Raman spectrum of (a) LPCVD grown monolayer graphene and (b) APCVD grown few-layer

graphene. (inset) Comparison of Raman profile of few-layer graphene with layer number from one to five and graphite at laser wavelength of 532nm.³⁰25

Figure 2-6. Illustration of the phonon vibration contributing to the (a) G band, (b) D and 2D band in graphene.³¹ Note that each abbreviation represents as follows: in-plane (i), transverse (T), longitudinal (L), optical (O).26

Figure 2-7. AFM height image of (a)-(b) monolayer graphene film (c)-(d) few-layer graphene film. AFM step height profile of (e) noticeable wrinkles in monolayer graphene and (f) a typical multi-layer region.27

Figure 2-8. SEM image of two types of graphene film on SiO₂/Si substrate for thickness, surface morphology and defects analysis. SEM images of monolayer graphene film at (a) 1.2kx, (b) 3.0kx magnification and of multilayer graphene film at (c) 1.24kx, (d) 2.37kx magnification. Note that EHT=5kV and In-Lens which is annular detector was used for all SEM images in this thesis.28

Figure 3-1. An overall process for transferring CVD-grown graphene by PMMA-mediated transfer, also referred to as the conventional wet transfer.32

Figure 3-2. (a) Schematic illustration of the PMMA-supported graphene transfer procedure onto a target substrate, representing the sequential steps after etching Cu foil. (b) OM image and (c) AFM image of transferred graphene film onto SiO₂/Si substrate which is corresponding to the last schematic in (a).33

Figure 3-3. (a) Schematic images of our PDMS/PMMA double-layer transfer method to transfer CVD-grown graphene onto desirable substrates.34

Figure 3-4. (a) Schematically illustrated our optimal PDMS/PMMA double-layer transfer process onto a target substrate, for CVD grown-2D materials which is following the etching of Cu substrate. Corresponding (b) OM image and (c) AFM image of transferred graphene film onto SiO₂/Si substrate...35

Figure 3-5. (a) (left) Cross-sectional image of the PDMS/PMMA/graphene film. The PDMS and PMMA layers play a role of an expandable and a gluing layer, respectively. Illustration of two possible reasons to reduce wrinkles in graphene, tensile stain aspect in upper-right side and adhesion energy aspect in bottom-right side. Note that interfacial tension (γ) values of PDMS, PMMA and graphene are 20, 38 and 62 mJ m⁻², respectively. (b) Comparison of film thickness of PMMA, PDMS and PDMS/PMMA double-layer.37

Figure 3-6. The AFM images of graphene transferred to a 300 nm SiO₂/Si substrate by using (a) the conventional PMMA-mediated and (b) the PDMS/PMMA double-layer transfer method. The corresponding AFM images and height profiles were taken with three different selected regions (red, blue, and black boxes). The wrinkle (c) height and (d) width distribution of graphene samples transferred by the conventional PMMA-mediated (black) and the PDMS/PMMA double-layer (red) transfer method. (e) Histograms of wrinkle density for the conventional PMMA-mediated (black) and the PDMS/PMMA

double-layer (red) transfer method. The wrinkles in $400 \mu\text{m}^2$ of graphene surface are counted. The indicated error bars of measurements are shown.39

Figure 3-7. Schematic process flow of wax-supported transfer method for CVD-grown monolayer graphene.41

Figure 3-8. Differential Scanning Calorimetry (DSC) thermal analysis of paraffin-wax which was used in our experiments, displaying thermal transition of the polymer.41

Figure 3-9. OM/SEM images of monolayer graphene on $\text{SiO}_2(300\text{nm})/\text{Si}$ wafer which was transferred via (a)/(c) the conventional wet transfer method and (b)/(d) our wax-supported transfer method, respectively.42

Figure 3-10. (a) Schematic illustration to describe the mechanism of our wax-mediated transfer method. Low magnification AFM height images of graphene film transferred by using (b) PMMA and (c) paraffin-wax. Corresponding high magnification AFM images of graphene by (d) PMMA-mediated transfer process and (e) wax-supported transfer process.44

Figure 3-11. The thermal expansion effects of paraffin-wax on monolayer graphene film with respect to temperature. The scale bars in (a)-(f) are all $5 \mu\text{m}$45

Figure 3-12. The AFM images of graphene transferred to a 300 nm SiO_2/Si substrate by using (a) the conventional PMMA-mediated and (b) the wax-mediated transfer methods. The corresponding AFM images and height profiles were taken with three different selected regions (red, blue, and black boxes). The wrinkle (c) height and (d) width distribution of graphene samples transferred by the conventional PMMA-mediated (black) and the wax-mediated (red) transfer method. (e) Histograms of wrinkle density for the conventional PMMA-mediated (black) and wax (red) transfer methods. The wrinkles in $400 \mu\text{m}^2$ of graphene surface are counted. The indicated error bars of measurements are shown.46

List of Tables

Table 1. Summary of some CVD growth works of graphene on Cu. ²¹	16
Table 2. Results of film thickness measured by a surface profiler.	37
Table 3. Comparison for chemical, physical and mechanical properties of PMMA and paraffin wax.	40

Chapter 1.

Introduction

1.1. Background

Novoselov *et al* reported a successful isolation of monolayer graphene (MLG), a free-standing two-dimensional sheet of carbon atoms, by mechanical cleavage of a highly ordered pyrolytic graphite (HOPG) and investigated the electric field effect in their samples in 2004.¹ Since the revolutionary work, both theoretical and experimental research on graphene has been widely conducted due to its exceptional physical properties such as extremely high carrier mobility in excess of $200,000 \text{ cm}^2 \text{ V}^{-1} \text{ s}^{-1}$,² quantum Hall effect,³⁻⁵ 97.7% transparency of visible light⁶ and ambipolar field effect⁷ which are attributed to the fact that electrons behave like massless Dirac fermions. The extraordinary properties of graphene have opened up many possibilities for new applications and systems including flexible electrochemical capacitors,⁷ stretchable transparent electrodes,⁸ high frequency electronic devices⁹ and gas sensors.¹⁰ This has rapidly aroused industrial as well as scholarly thrust because graphene would be a promising candidate to overcome current limitations of practical applications. To satisfy these industrial demands, a high quality homogeneous wafer-scale graphene is required to fabricate integrated devices in a fashion compatible with the existing deposition processes. Therefore, it is highly desirable to develop synthesis methods to obtain large size graphene with reasonably high quality.

There are two approaches to prepare graphene samples which are either top-down or bottom-up processing. We can obtain micron-size graphene flakes from a bulk graphite by mechanical as well as chemical exfoliation (top-down methods). It is attributed to the fact that the layered crystal consists of atomically thin monolayers with weak van der Waals bonding between layers. Although a simple mechanical exfoliation method¹¹ allows us to study physical fundamentals with the best quality graphene with low concentration of structural defects, the top down method is unfavorable because it lacks control of the number of layers, flakes size and the locations of the graphene flakes, limiting their practical applications. One strategy to achieve scalable and reproducible graphene is the epitaxial graphene growth on single crystal SiC (0001) via sublimation of silicon atoms at high temperatures in ultrahigh vacuum conditions¹¹. However,

the SiC wafer is very expensive compared to the price of a silicon wafer so there is a cost factor in this growth method. Another example to address scalability issues is chemical exfoliation techniques which disperse and exfoliate graphite in liquids by taking advantage of weak van der Waals bonding. Despite low cost and ease in scaling up, these methods create structural and electronic disorder during reduction and oxidation processes which causes large deviation of electronic properties from those of intrinsic graphene¹² leading to degradation of electrical properties and thus device performances. With these reasons, the chemically derived graphene thin films cannot be used for high performance device applications.¹³

There also would be possible to synthesize large area of graphene by using standard chemical growth techniques. Those bottom-up method to chemically grow graphene are an area of rapid progress nowadays. Among them, chemical vapor deposition (CVD) has been a focus of attention as the most promising and cost-efficient deposition techniques, with advantages of its excellent repeatability and controllability, to produce large area graphene crystals on transition metal catalyst substrates such as copper (Cu) or nickel (Ni). In particular, Cu with low carbon solid solubility leads to uniform single layer deposition of graphene over large areas.^{14,15} The CVD grown graphene films exhibits low sheet resistances of $< 1 \text{ k}\Omega/\text{sq}$, high carrier mobility ($2000\sim 4000 \text{ cm}^2 \text{ V}^{-1} \text{ s}^{-1}$) and more than 90% optical transparency.^{8,16} However, these CVD grown graphene are generally inferior compared to mechanical exfoliated single layer of graphene due to its poly crystallinity. Additionally, subsequent transfer processes to target substrates from the metal substrate are necessary for electronic applications. The transfer process usually gives rise to deterioration of the graphene quality.

In this regard, both growth and transfer processes should be considered carefully, with deep understandings of structural disorder, to improve the performance of CVD-grown graphene that is comparable to mechanical exfoliated ones. Several groups have already reported large area graphene films and devices of outstanding performance.^{15,17} For example, Li *et al* achieved graphene films with large domain size by optimizing growth parameters of a two-step CVD process, and demonstrated back-gated field effect transistor (FET) with high carrier mobility up to about $16,000 \text{ cm}^2 \text{ V}^{-1} \text{ s}^{-1}$ at room temperature.¹⁷ Thus, there are great potential for synthesizing high quality of graphene over large area by CVD which can satisfy the industrial needs.

1.2. Electronic structure of graphene and its properties

Graphene, an atomically thin single layer of carbon atoms densely packed in a hexagonal crystal lattice as shown in figure 1-1, has been a center of attention because it displays a high crystalline quality and charge carriers behave like massless relativistic particles in graphene.^{18,19} The two-dimensional Dirac fermions can be controlled by modifying topology and geometry of the samples or applying magnetic and electric fields. Furthermore, the electronic properties of graphene are strongly dependent on the number of layers, stacking order, boundary conditions and overall quality of crystal lattice including various types of defects. For example, the electronic properties are significantly different in zigzag edges and armchair edges. Graphene is comprised of sp^2 hybridized carbon atoms with interatomic spacing of 1.412 Å. The one s orbital and two p atomic orbitals on each carbon atom form strong covalent σ bond which contributes to high Young's modulus of ~ 1 TPa and a trigonal planar structure. The σ bands are fully occupied so that they form a deep valence band. The remaining p_z orbital that is perpendicular to the carbon lattice plane forms half-filled π band by binding with neighboring p_z orbitals. Based on calculation from tight binding model, the π band consists of two energy bands which are a valence band of filled π orbitals and a conduction band of empty π^* orbitals. Electrons in the π band are delocalized. This is responsible for charge carriers transport in graphene, which gives rise to electrical conductivities in the in-plane direction.

According to the electronic dispersion curve shown in figure. 1-1 (c)²⁰, the π bands cross at two Dirac points (also, neutral points) $K = (\frac{2\pi}{3a}, \frac{2\pi}{3\sqrt{3}a})$ and $K' = (\frac{2\pi}{3a}, -\frac{2\pi}{3\sqrt{3}a})$ of the corners of the Brillouin zone, which is the origin of zero-band gap in graphene. Therefore, graphene shows a linear dispersion relation close to the Dirac points as given by

$$E = \hbar v_f |k|,$$

where v_f (Fermi velocity) $\approx 10^6$ ms⁻¹ estimated by fitting an equation to the experimental data

$$m^* = \frac{\sqrt{\pi}}{v_f} \sqrt{n},$$

where m^* is a cyclotron mass and n is an electronic density.¹⁸ The density of states in 2D space can be described as

$$g(E) = \frac{2E}{\pi \hbar^2 v_f^2},$$

where $E > 0$.

Given the unique band structure, graphene shows a semi-metallic behavior and has a zero-effective mass for both the electron and hole carriers near at the Dirac points. Thus, charge carriers can propagate with minimal optical phonon scattering over large distances.

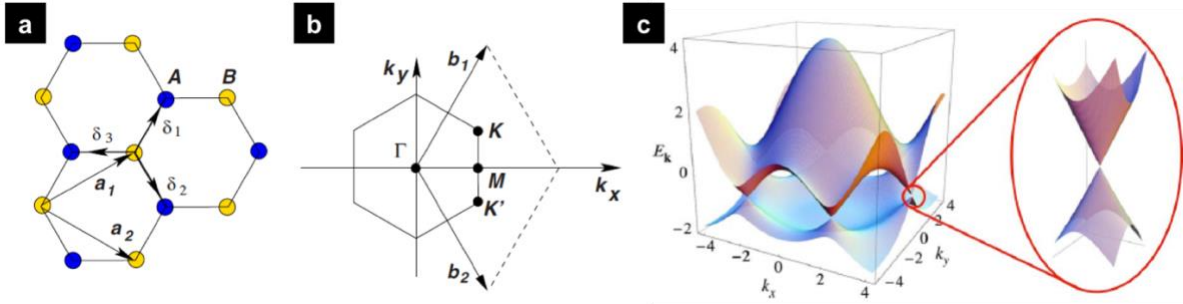


Figure 1-1. Schematics of hexagonal crystal lattice and its corresponding Brillouin zone.

(a) Honeycomb lattice structure of graphene with two atoms per unit cell, representing inequivalent carbon atoms A (blue) and B (yellow), the lattice unit vectors, \vec{a}_1 and \vec{a}_2 and the nearest-neighbor vectors, $\vec{\delta}_1$, $\vec{\delta}_2$, and $\vec{\delta}_3$. (b) Construction of first Brillouin zone of graphene, showing two distinct Dirac points K and K' , high symmetry points Γ , K , and M and the unit vectors in reciprocal space, \vec{b}_1 and \vec{b}_2 . (c) $E(k)$ dispersion curve of graphene for finite values of t and t' , with $t=2.7\text{eV}$ (the nearest-neighbor hopping energy) and $t'=-0.2t$ (the next nearest-neighbor hopping energy). Zoom in energy band structure close to one Dirac point (red circle).¹⁹

1.3. Graphene growth on transition metal substrates

Although catalyst-assisted synthesis of graphene in a thermal CVD process has been relatively new, graphene growth on metal substrates such nickel(Ni)⁸, copper(Cu)¹⁴ and ruthenium(Ru)²⁰ via thermal CVD process is attracting intensive attention because it can help in realizing the large area high quality graphene with good uniformity in a cost-effective and simple manners. The transition metals play a key role as catalysts to decompose the hydrocarbon sources. Since the growth mechanism relies on the type of substrates, the suitable metal substrate can be chosen for purpose.

Even though a great variety of metal substrates are available, inexpensive polycrystalline Cu and Ni substrates have been mainly studied to realize large area deposition. It has been shown that Cu foil is very useful to prepare high quality monolayer graphene due to its negligible carbon solubility (<0.001 atomic %) at around 1000°C, limiting the deposition of carbon species to the Cu

surface. On the other hand, Ni exhibits a high carbon diffusivity and a good carbon solubility as function of temperature (see figure 1-2 (a)) so that graphene forms via two steps: (1) decomposed carbon atoms diffuse into the Ni thin film at high growth temperature (~1000 °C), (2) carbon atoms precipitates on the metal surface by diffusing out from the bulk substrate upon cooling to room temperature after CVD growth.¹⁶ Thus, single- to few-layers graphene film can be synthesized on a polycrystalline Ni substrate through an atmospheric CVD (APCVD) method.^{8,16} It has been found that the thickness and crystalline ordering of graphene thin film is determined by the carbon concentration in the bulk Ni, the cooling rate and the thickness of the Ni film. It is, however, still challenging to get homogenously continuous graphene film with high quality due to the limitations: (1) graphene is deposited over few to tens of microns, (2) multilayers present at grain boundaries because highly dissolved carbon in Ni preferentially precipitates out at the grain boundaries of Ni.

Contrary to growth on Ni film, as aforementioned briefly, graphene synthesized on polycrystalline Cu foil has exceptional film uniformity over large area. It has been demonstrated that monolayer graphene was grown over 95% of the Cu surface while few layers graphene covered the remaining surface.¹⁴ With the benefit of low carbon solubility in Cu, the growth mechanism is simpler. The process is carried out as a self-limiting process which is a surface-catalyzed process. Methane gas, one of carbonaceous gas, has been commonly used for graphene growth under both atmospheric and low (500mTorr ~ 50Torr) pressure. It decomposes over a Cu surface at around 1000 °C at where the carbon solubility of Cu is approximately ~0.0006 at% as described in figure 1-2 (b). Table 1 provides reported growth conditions of high quality graphene thin film on Cu substrates according to several growth parameters such as temperature, pressure, annealing condition, growth time, cooling rate, hydrogen and methane flow ratio and thickness of Cu film.²¹ Liquid precursors, such as Hexane, have also been reported to get homogenous single- to few-layer graphene on a Cu substrate at 950 °C. The liquid precursor based growth takes advantage of easy doping in graphene because organic solvents can contain dopant atoms such as nitrogen and boron.²²

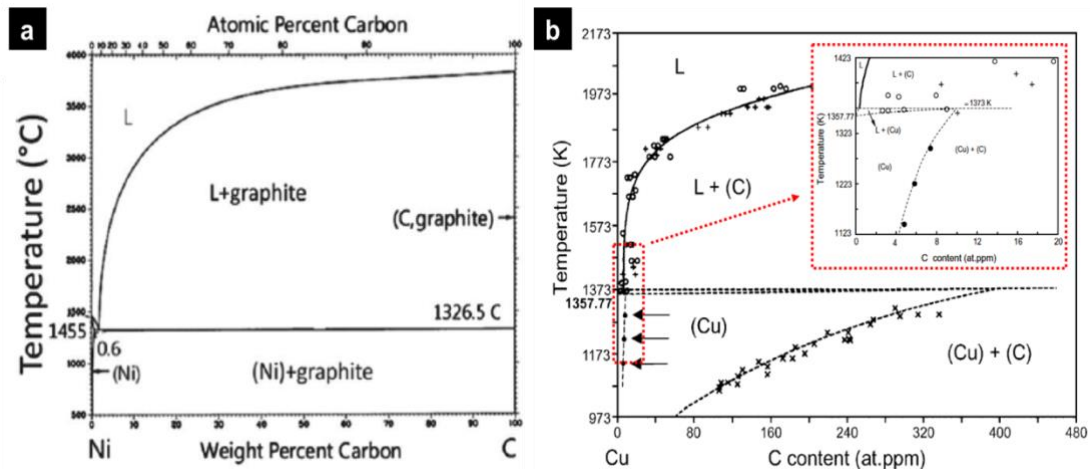


Figure 1-2. Equilibrium phase diagram of (a) Ni-C binary system;²¹ (b) Cu-C binary system; (inset) zoom-in of Cu-C binary phase diagram at the Cu-rich region.²³

At 1000 °C, the carbon solubility (a) in Ni is ~ 1.1at%, (b) in Cu is ~ 0.0006at%.

Growth Pressure (Torr)	Pre-annealing	H ₂ /CH ₄ flow ratio (sccm), growth time and cooling rate	Temperature (°C)	Cu Thickness	#Graphene layers
0.5	1000 °C H ₂ (2 sccm, 0.04 Torr) 30 min	0.06 (1min–60 min, cooling rate 40–300 °C/min)	1000	25 μm	>95% 1
11	(base pressure 0.1Torr) Acetic acid + heating up to 1000 °C H ₂ (50–200 sccm, 2 Torr 40 °C/min)	0.23 (10–20min, cooling rate 20 °C/min + gas flow)	1000	500 nm and C foil 25 μm	>93% 1
50	900 °C 30 min H ₂ 10 Torr	10Torr/40Torr (10 min, cooling rate 10 °C/s) CH ₄ (99.999%)	850–900	50 μm	Few layers
760	1. Heating up to 1000 °C in ambient pressure. 2. 30 min, 1000 °C He(1000sccm) + H ₂ (50sccm)	15 : 50 : 1000 sccm (H ₂ :CH ₄ :He) (5min, cooling rate in He 10 °C/s)	1000	700 nm	1,2
0.39	1. Ar (20sccm, 0.41Torr 12 min), 2. H ₂ (20sccm, 0.3Torr 1.25 min) up to 766 °C	5 (10 min) cooling in Ar 80 sccm 1Torr	800	206 nm	1,2,3
0.1–0.5	(pre-vacuum) Heating in H ₂ up to 1000 °C	0.06 (from 15 min up to 420 min) CH ₄ (99.99%)	1000	100–450 nm	1
0.5	(pre-vacuum 0.01) Ar/H ₂ 400 sccm 8–9 Torr up to 950 °C	Hexane (4mL/h) 4 min	950	25 μm	1,2
0.3	(pre-vacuum) Heating up to 1000 °C H ₂ (13 sccm, 0.1 Torr) 30 min	0.5 (30 s–30min) cooling rate 9 °C/min	1000	25 μm, 125 μm	1,2
1.6	Heating up to 1000 °C H ₂ (8 sccm, 0.18 Torr) 30 min	0.33 (30 min) (cooling rate 10 °C/s, H ₂ 0.18 Torr)	1000	25 μm	1

Table 1. Summary of some CVD growth works of graphene on Cu.²¹

1.4. Transfer process of CVD-grown graphene

Centimeter-scale single crystalline graphene has been successfully synthesized by CVD process²⁴, which has allowed graphene to be used for practical applications. In CVD process, the metal substrates are necessary to catalyze the CVD growth of graphene which means that a subsequent transfer process to a substrate of interest is required for a wide variety of applications, especially in electronics and photonics. It is important not only to improve quality of as-grown

graphene by optimizing the growth conditions but also to develop transfer methods to prevent degradation in quality while transferring as-grown graphene to target substrates. In the case of wet transfer, surface tension of the liquid such as the etching solution or water contributes to form inevitable ripples, wrinkles and cracks. In order to maintain the integrity of graphene during the transfer process, a protective layer (also known as supporting layer or sacrificial layer) on top of the graphene surface is needed. There are several requirements of this polymeric support layer. The carrier layer should have both of the low adsorption energy with the graphene surface and good solubility in solvents which makes the polymer be easily removed from graphene without leaving residues and damages. It also should have high mechanical robustness to support the graphene film as well as a reasonable flexibility to form conformal contact with the graphene. Lastly, it should have strong resistance to metal etchants. Under such conditions, polymer has been found to be as very suitable candidate.

The most common supporting polymeric material is poly (methyl methacrylate) (PMMA) which is a flexible thin film. However, it has been found that the PMMA layer leaves residues in graphene. It attributes to several physical properties of PMMA: (1) strong interaction with graphene due to large adsorption energy with graphene surface, (2) low solubility in organic solvent. For these reasons, discovering new supporting materials has been of great importance. For example, Zhang *et al* reported the transfer method based on rosin that they embodied flexible organic light-emitting diode (OLED) with a high luminance of 10,000 cd m⁻² by utilizing cleaner and damage-free graphene.²⁵ (See figure 1-3) With the effort to find suitable support layers, drawbacks of polymer-based transfer method which is non-scalable and non-integratable with synthesis process need to be improved through other transfer method like a roll-to-roll process.

1.5. Thesis objectives

This thesis aims to investigate either of mono- and few-layers graphene growth by CVD method and present novel transfer techniques in order to significantly reduce density of defects, wrinkles and residues, which makes our CVD-grown graphene more suitable for electronics and other practical applications such as membrane. This thesis is mainly composed of two parts: synthesis and transfer. Specifically, this is organized as follows: Chapter 2 covers the synthesis part, either mono- or few-layer graphene growth on Cu foil are explored. Their film qualities are

investigated by various characterization techniques, for example optical microscopy, Raman spectroscopy, atomic force microscopy, scanning electron microscope and ultraviolet-visible spectroscopy. Chapter 3 covers the investigation on transfer processes for graphene and universal 2D materials. I will introduce two different transfer methods but their basic concept is quite similar which minimizing wrinkles by employing thermal strain. Finally, chapter 4 provides a summary of our works performed in this thesis.

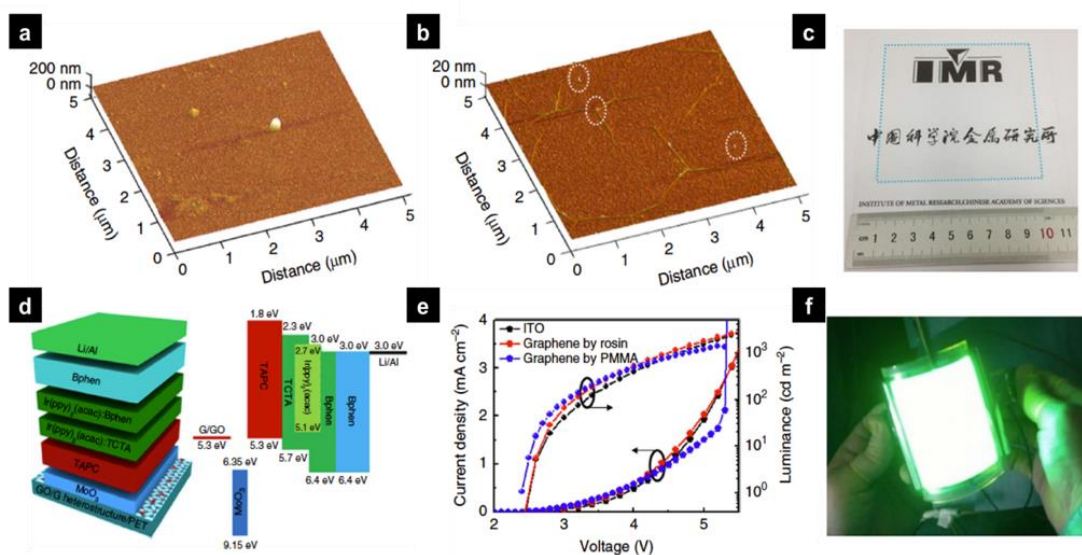


Figure 1-3. Surface roughness characterization, optical properties of graphene transferred by using different supporting materials. Graphene-based OLED.

AFM images of (a) PMMA- and (b) rosin-mediated graphene. Small rosin residue particles are marked as the white circles. (c) a monolayer graphene film (blue dot square) with the size of 10 x 10 cm² onto a polyethylene terephthalate (PET) film. (d) schematic of OLED device structure (left) and its energy band diagram (right). (e) plot of current intensity and luminance versus voltage respectively. (f) photo of large area flexible green OLED with a rosin-transferred five-layer graphene anode.²⁵

Chapter 2.

CVD growth of graphene

2.1. Synthesis of graphene on a Cu foil

In the following sections, the synthesis methods based on CVD to grow high-quality continuous films of single- and few-layer graphene are demonstrated with a Cu foil as a metal catalytic substrate.

As mentioned earlier, we have decided on a Cu foil as a catalyst because a Cu foil has been regarded as the most common substrate to grow homogeneous single-layer graphene due to its low carbon solid solubility below or at growth temperature. The CVD growth of monolayer graphene usually consists of four consecutive steps as follows; heating, thermal annealing, growth and cooling process. First of all, the bulk Cu foil is heated up to growth temperature which is typically ~ 1000 °C where hydrocarbon source is able to be decomposed. While thermally annealing the substrates, a native oxide layer on the Cu foil is removed under hydrogen gas atmosphere. Simultaneously, the grain size of the Cu gets bigger and the surface morphology smoothens at the high annealing temperature. In the subsequent growth stage, carbonaceous gas is introduced into the CVD system as a precursor. Once the growth step is finished, the CVD furnace is naturally cooled down to room temperature with flow of hydrogen and hydrocarbon gas.

2.1.1. Chemical pretreatment of Cu foil

We have studied the effects of various pretreatment methods on the surface morphology of Cu substrate by using scanning electron microscopy (SEM), in order to make the inconsistent rough surface to a relatively flat surface prior to the CVD growth of graphene. This is because both the growth mechanism and quality of graphene is dependent on the surface condition of the Cu foil. In general, the surface morphology and the amount of impurity particles of native Cu thick films are very different from batches to batches and by suppliers using different manufacturing process. This makes it hard to obtain homogenous monolayer graphene with reproducibility due to the fact that the impurity particles (mostly metal particles such as Si, Pt, Ru and Ca etc.) and

steps on the Cu surface play a role of preferable nucleation sites promoting multilayer growth. To exclude the influence arising from Cu foil and increase the reproducibility of growth process, the most frequently way of use is a pre-cleaning of the Cu foil with acidic or basic solutions such as acetic acid, hydrochloric acid, nitric acid, chromium etchant and sodium hydroxide.²⁶

In our experiments, acetic acid (glacial, VWR Scientific) and Ni etchant (Transense) were used to clean the Cu foil. Figure 2.1 shows a comparison of pretreatment methods between acetic acid and Ni etchant. (a) and (c) are surface morphology images recorded with SEM when using acetic acid. (b) and (d) shows the SEM images of Cu surface after pre-cleaning with nitric acid. We examined the cleaning effect by using Cu foil from the same batch and the same company (Alfa Aesar). One foil was dipped in acetic acid for 6 hours and the other one was soaked in nitric acid for 90 seconds in a bath-sonicator. For both cases, washing processes with deionized (DI) water were followed to remove the acid.

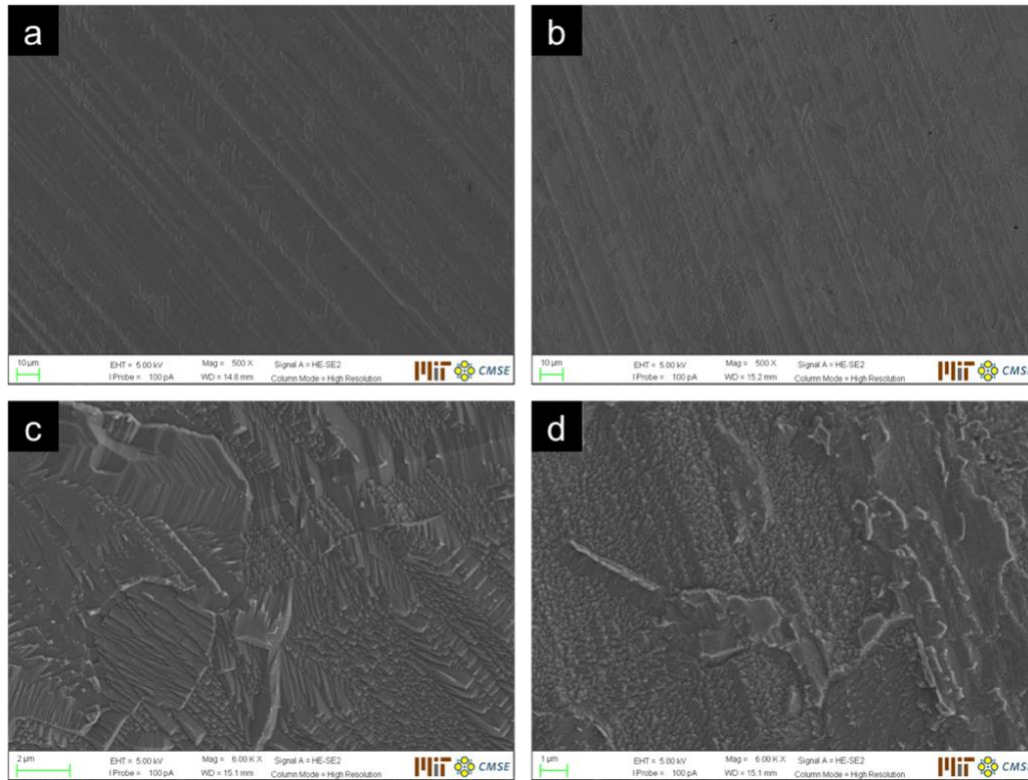


Figure 2-1. Scanning Electron Microscope (SEM) images of a Cu foil with respect to different pre-cleaning methods.

SEM images of the Cu surface chemically treated with (a)(c) acetic acid and (b)(d) nickel etchant in different magnification of (a)-(b) x500 and (c)-(d) x6000.

2.1.2. Monolayer graphene by Low Pressure CVD (LPCVD)

In this work, the synthesis of monolayer graphene was performed by low pressure chemical vapor deposition (LPCVD) according to the temperature-time profile as shown in figure 2-2. A tubular quartz tube with 1-inch diameter was used in the CVD system to grow monolayer graphene on 25 μm thick Cu foil purchased from Alfa Aesar (99.8%, #13382). Before graphene growth, the Cu foils were pre-cleaned with the Ni etchant (Transense) to remove common impurity particles on the foils which allowed us to obtain a clean, continuous and high quality of monolayer graphene. The pre-treated Cu foil was placed in a CVD quartz chamber and was heated up to the growth temperature. After the temperature is stabilized, the Cu foil was annealed under a pressure of 1.5 Torr with a flow rate of 50 standard cubic centimeters (sccm) of hydrogen gas (H_2) at 1035 $^\circ\text{C}$ for 1 hour, which allowed to increase the Cu grain size and smoothen the surface. It should be noted that H_2 functions as not only an etching agent limiting the formation of amorphous carbon with dangling bonds but also it plays a major role for CVD diamond growth.²⁷ During the growth period, 6 sccm of methane (CH_4) gas was introduced at 1035 $^\circ\text{C}$ for 40 min. The graphene growth was carried out in a flow rate of 40 sccm of H_2 to control the graphene growth rate. After the CVD reaction, the LPCVD system was cooled down to room temperature under 40 sccm of H_2 and 6 sccm of CH_4 to keep from oxidizing and to minimize hydrogenation reactions of the graphene.

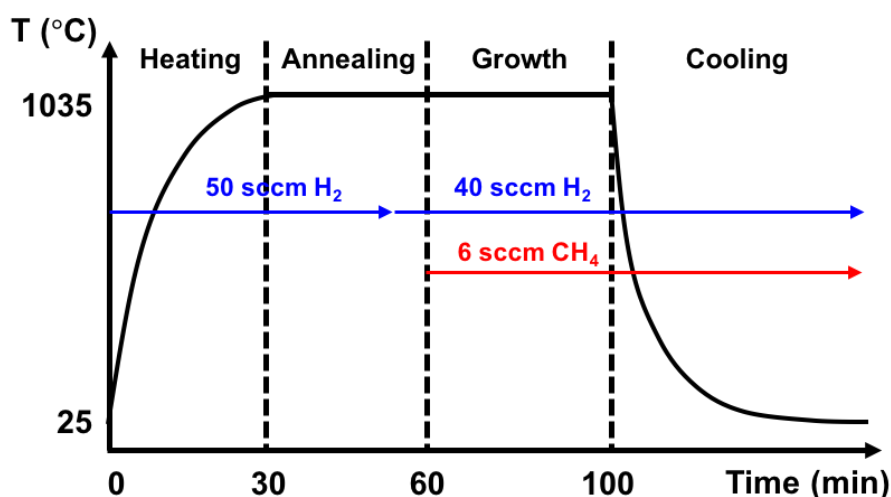


Figure 2-2. A schematic flow of single layer graphene growth by CVD system, illustrating the temperature profile as a function of time.

2.1.3. Multilayer graphene by Ambient Pressure CVD (APCVD)

Multilayer graphene was synthesized under ambient pressure CVD system (APCVD) using a gas mixture of argon (Ar), H₂, and CH₄. It has been found that APCVD growth process is not self-limiting so it can be used to get multilayer graphene rather than monolayer graphene. Under the same experimental condition, the Cu foil and pretreatment process using Ni etchant, the Cu foil was positioned at the center of a quartz tube and was heated up to 1000 °C at a ~17°C/min heating rate under the flow of 1000 sccm Ar. Once the temperature was stabilized, H₂ was introduced in the furnace and the Cu foil was kept at 1000°C with the gas flow of Ar:H₂=1000:300 sccm for 30 min to anneal the metal substrate. Subsequently, 10 sccm of methane (CH₄) gas was introduced at 1000 °C for 15 mins while synthesizing the multilayer graphene. As soon as the growth process was completed, the sample in the quartz tube was naturally cooled down to room temperature under a flow of gas mixture consisted of Ar: H₂: CH₄=1000:300:10 sccm. The detailed description of the growth condition is as illustrated in figure 2-3.

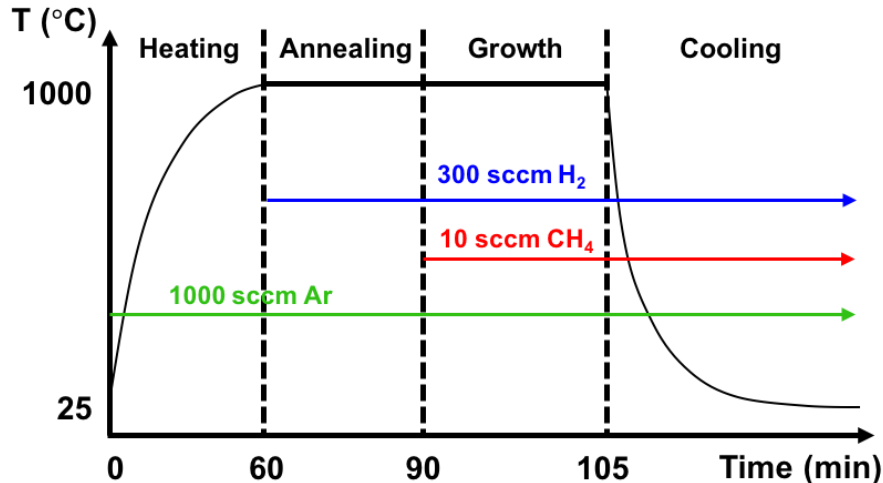


Figure 2-3. A schematic flow of multi-layer graphene growth by CVD system, representing the temperature profile as a function of time.

2.2. Characterizations

Here, we have extensively investigated the film quality of CVD-grown graphene through various characterization techniques: optical microscopy (OM), Raman spectroscopy, atomic force microscope (AFM), scanning electron spectroscopy (SEM), Hall measurement and ultraviolet-visible spectroscopy.

2.2.1. Optical Microscopy (OM)

In both cases of mono- and few-layer graphene, the Cu foil were fully covered with CVD grown graphene, respectively. The continuous area of the films grown in this work is typically ~ 2 cm x 10 cm (also same as Cu foil size) which is limited by the dimension of the 1-inch wide quartz tube of our CVD system. The mono- and few-layer graphene were transferred onto SiO₂(300nm)/Si wafers from the Cu surface to explore their OM images, which allowed us to evaluate the thickness uniformity and continuity of the film as well as residues, defects and broken region on the film in detail. Additionally, OM was also used to characterize the layer distribution of the few-layer graphene sheet on the wafer based on apparent color contrast of different regions. In figure 2-4 (a), we observed the incomplete and partially grown graphene film made of many star-shaped (also known as lobe-shaped dendritic morphology) small domains. This suggests that growth time was not enough to form continuous graphene film. Under the circumstance of enough growth time, homogenous high-quality monolayer graphene film was synthesized as shown in figure 2-4 (b) and (c). Even though it was clean and uniform over the whole region, polymer residues and wrinkles were still found in the film. This issue will be further discussed in the later chapter of the thesis. As can be seen in figure 2-4 (d), completely continuous multi-layer graphene was successfully synthesized by APCVD system. The darker region corresponds to thicker layers. Such few-layer graphene was also transferred onto borosilicate glass in order to check transmittance of the film. With ultraviolet-visible (UV-Visible) spectroscopy, the optical transmittance of the few-layer graphene was measured to be $\sim 88\%$. We could assume that the number of layers would be less than 10 layers when compared to simulation results.²⁸ The few-layer graphene has exhibited better mechanical robustness than monolayer graphene. It is probable that the few layer regions help to stitch the monolayer regions, preventing disruption or breaking in the graphene.

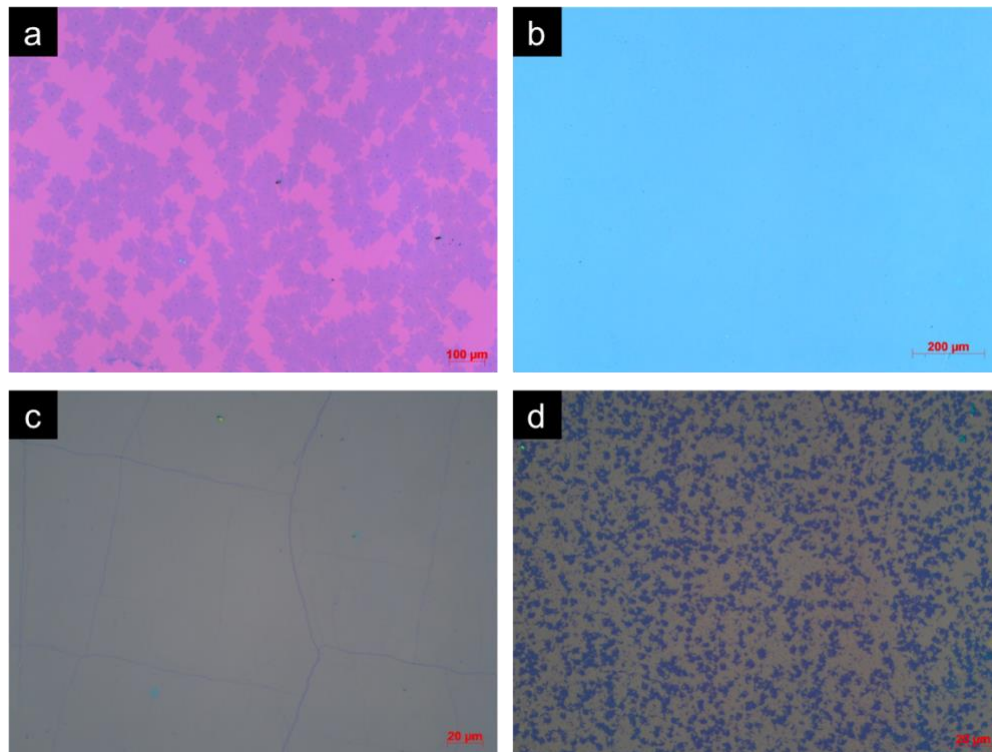


Figure 2-4. Optical Microscopy (OM) images of a CVD-grown graphene sheet on SiO₂/Si wafers.

OM image of a monolayer graphene film (a) before the formation of a continuous film. (b) a low magnification and (c) a high magnification OM images of homogenous and continuous film. (d) OM images of a few-layer graphene film.

2.2.2. Raman spectroscopy

Raman spectroscopy is a powerful tool for characterizing 2D materials including graphene. It has been universally used to study the number of graphene layers, evaluate the presence of defects and doping or strain in graphene, and also the stacking order of bilayer graphene. As can be seen in figure 2-5 (a), the CVD-grown monolayer graphene film exhibits two most intensive Raman modes and another disorder-related peak: a doubly-degenerate in-plane sp² C-C stretching mode (G band) at ~1580 cm⁻¹ which is first order Raman process, an in-plane breathing-like mode of hexagon ring consisting of six carbon atoms (2D band) at ~ 2700 cm⁻¹ which is also referred to as a second order Raman mode, the disorder-related mode (D band) at ~1350 cm⁻¹ (see figure 2-6), induced by the symmetry breaking in graphene lattice such as point defects, edges, grain boundaries or impurities. We could measure the deformation and strain from the width of G peak because the two-degenerate modes start to split into the G⁺ and G⁻ band under deformation.²⁹ The

number of graphene layers could be determined through the 2D band, this peak can dissociate into several peaks when the graphene is not a single-layer. The Raman spectrum in figure 2-5 (b) shows broad 2D peak comprised of several sharp peaks, which evidences the existence of multi-layer graphene. Specifically, one sharp 2D peak becomes the superposed four sub-2D bands by the addition of the second layer, leading to the increase in the bandwidth. The ratio between the intensities of the 2D and G bands (I_{2D}/I_G) can be indicative of the number of graphene layers as well, it has a tendency of decreasing as the number of layers increase. But, the intensity ratio is also linked to disorder and the doping so that the shape of 2D band is a more reliable estimation of the layer thickness.

In the figure 2-5 (a), the confocal Raman spectra of our CVD-grown monolayer graphene showed relatively high I_{2D}/I_G and sharp 2D band, reflecting the fact that the region under examination is monolayer. The D peak suggest the presence of defects in the graphene.

The multilayer graphene was also characterized by Raman and the spectra were shown in figure 2-5 (b). It shows low I_{2D}/I_G intensity ratio and a broad 2D band. These suggest optimization on CVD-grown few-layer graphene is inevitable in the near future.

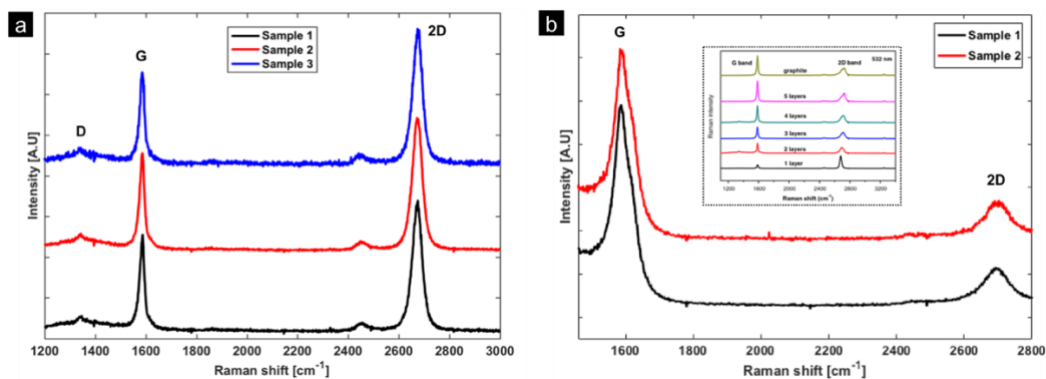


Figure 2-5. Raman spectroscopy obtained from a CVD-grown graphene after transferred onto the SiO_2/Si wafer.

Raman spectrum of (a) LPCVD grown monolayer graphene and (b) APCVD grown few-layer graphene. (inset) Comparison of Raman profile of few-layer graphene with layer number from one to five and graphite at laser wavelength of 532nm.³⁰

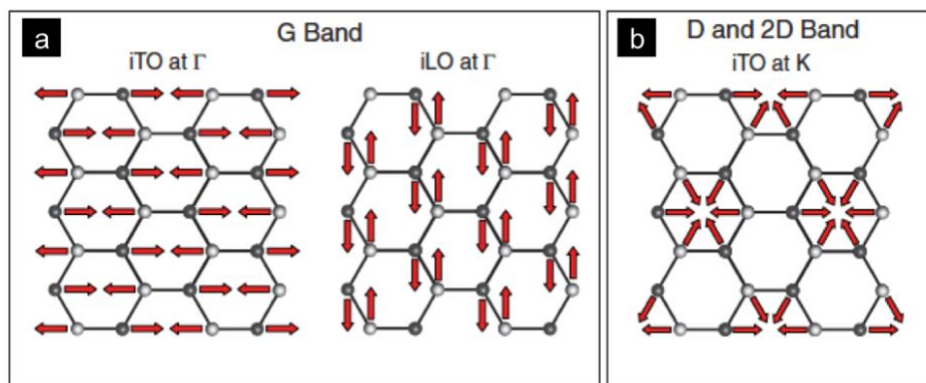


Figure 2-6. Illustration of the phonon vibration contributing to the (a) G band, (b) D and 2D band in graphene.³¹

Note that each abbreviation represents as follows: in-plane (i), transverse (T), longitudinal (L), optical (O).

2.2.3. Atomic Force Microscopy (AFM)

Figure 2.7 shows the AFM images of CVD grown monolayer graphene and few-layer graphene on SiO₂/Si substrate. Wrinkles of monolayer graphene and few-layer graphene domains can be clearly observed in figure 2.7 (a) and (c), respectively. The heights of wrinkles on monolayer graphene is approximately 2.8 nm (RMS: 1.241nm \pm 0.56 nm) as described in figure 2-7 (e). These wrinkles could arise from the difference between thermal expansion coefficient between graphene and Cu foil during the growth process or forces during the transfer of graphene onto the target substrate. The thickness of few-layer graphene domain on fully covered monolayer graphene as measured by AFM was 4 nm. (figure 2-7 (f)). Compared with experimental value in literature³², we could estimate that the multilayer domain was comprised of 10 layers stacked vertically.

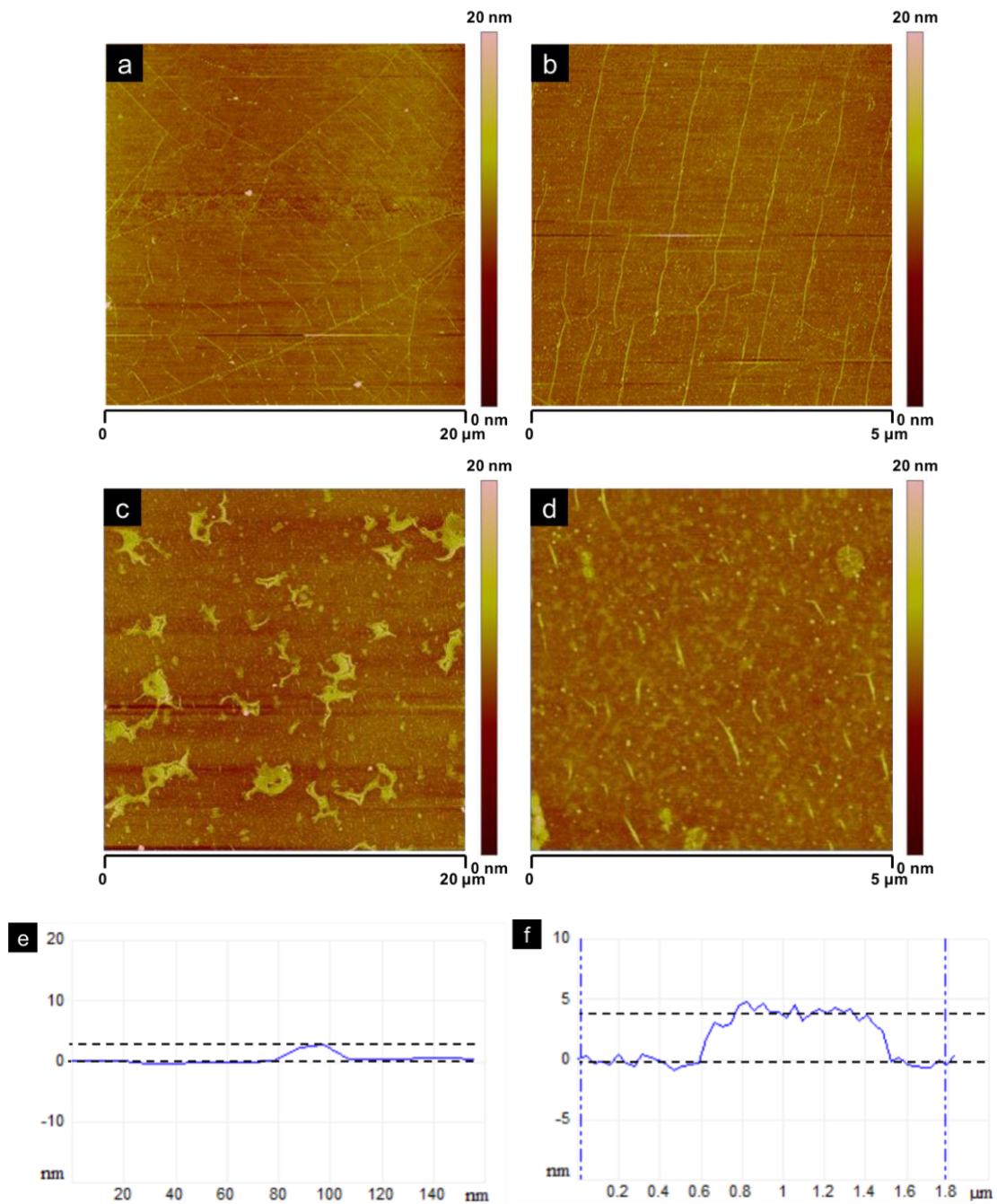


Figure 2-7. AFM height image of (a)-(b) monolayer graphene film (c)-(d) few-layer graphene film. AFM step height profile of (e) noticeable wrinkles in monolayer graphene and (f) a typical multi-layer region.

2.2.4. Scanning Electron Microscope (SEM)

The SEM images of CVD-grown graphene are shown in figure 2-8. In the case of monolayer graphene, it is continuous and homogenous but the wrinkles are also clearly visible. (figure 2-8 (a)-(b)). Whether it is large or small wrinkles, they are formed during the growth and the transfer process as described in the earlier section. The small bright/dark spots and dots show the presence of external impurities (such as Si or metal atoms) and polymer residues.

The SEM images (figure 2-8 (c)-(d)) shows multilayer graphene regions are grown on a monolayer background. The thickness of the multilayer graphene is not homogenous that the darker region corresponds to the thicker regions. The boundaries between multilayer domains and monolayer graphene are sharp enough to observe. Bright dots corresponding to residues and impurities were also seen.

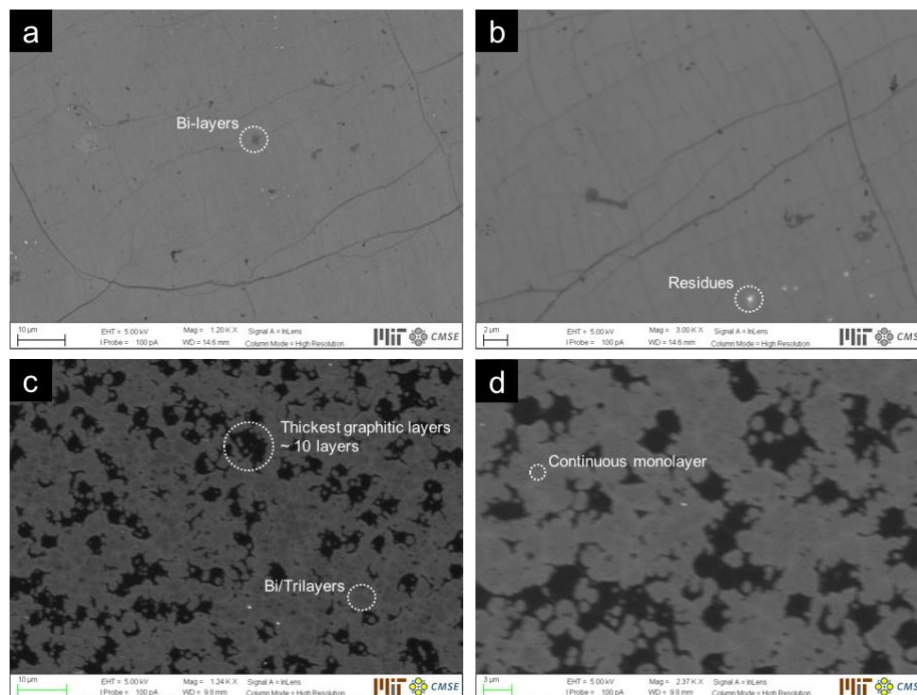


Figure 2-8. SEM image of two types of graphene film on SiO₂/Si substrate for thickness, surface morphology and defects analysis.

SEM images of monolayer graphene film at (a) 1.2kx, (b) 3.0kx magnification and of multilayer graphene film at (c) 1.24kx, (d) 2.37kx magnification. Note that EHT=5kV and In-Lens which is annular detector was used for all SEM images in this thesis.

2.2.5. Hall measurement

Here, we investigate electrical properties of the CVD-grown single-layer graphene. In particular, Hall mobility (μ_{Hall}) and sheet resistance (R_s) were extracted through the Van der Pauw method (also known as a four-point probe measurement). The 10 monolayer graphene films with geometry of 1 cm x 1cm square were measured to get those electrical characteristics. Silver paste was used as a contact electrode. The value of μ_{Hall} , $2184.625 \pm 266 \text{ cm}^2 \text{ V}^{-1} \text{ S}^{-1}$ was obtained in the poly-crystalline continuous single layer graphene film. The R_s of those samples were $480.1 \pm 65.03 \text{ } \Omega/\text{sq}$ which is quite reasonable value in a polycrystalline and un-doped monolayer graphene samples.

Chapter 3.

Transfer process for graphene

3.1. Background

An essential prerequisite for practical applications is the development of reliable synthetic method for large area of the high quality thin films. Chemical vapor deposition (CVD) method has been recognized as one of the most important and reliable techniques to produce large-area, high-quality of graphene, but also other 2D materials. This bottom-up method offers a compromise between quality, efficiency, consistency, and control over the process by precisely adjusting the growth temperature, growth time, quenching rate and the ratio of gas mixture.

However, the CVD grown 2D material, which is transferred onto target substrate of plastic, glass or oxide layer on silicon, suffers from the presence of localized structural defects, such as intrinsic ripples, extrinsic wrinkles and cracks. In particular, wrinkle formation has been observed ubiquitously in CVD graphene and received considerable attention because these wrinkles cause the degradation of graphene quality. It is believed that the coefficient of thermal expansion (CTE) mismatch between the graphene and the underling metal substrates is the main cause for the wrinkle formation during cooling. To be specific, wrinkle formation mechanism for graphene on poly-nickel foil has been investigated that the wrinkles are generated on the step edges between Ni terraces by nucleating defect lines and then grow due to thermal stress induced by the CTE difference between graphene and Ni foil. The CTE values of metal substrates (*e. g.* 16.6, 13.0 and $9.0 \times 10^{-6} \text{ K}^{-1}$ for Cu, Ni and Pt, respectively) are much higher than that of graphene ($-7 \times 10^{-6} \text{ K}^{-1}$), leading to the fact that graphene grown on metal substrates incorporate compressive stresses, resulting in the formation of localized wrinkles.

It has been reported that wrinkles, mechanical deformations in the graphene film, degrade the electrical and physical properties of the graphene, so most of the CVD-grown graphene show an inferior performance than in the exfoliated graphene. For example, the CVD-grown graphene exhibits the reduced carrier mobility compared to the higher mobility of the exfoliated graphene ($>10 \text{ m}^2 \text{ V}^{-1} \text{ s}^{-1}$). Bolotin *et al* have obtained mobility values more than $200,000 \text{ cm}^2 \text{ V}^{-1} \text{ s}^{-1}$ at electron densities of $\sim 2 \times 10^{11} \text{ cm}^{-2}$ from a mechanically exfoliated single layer graphene flake

with a suspended graphene device.² This is due to the fact that the wrinkles and domain boundaries tend to act as charge carriers scattering centers, and the carbon atoms along the wrinkle are found to be less stable due to the curvature effect. Moreover, it has recently found that wrinkles and defects in the graphene film are preferential failure sites in nano-porous graphene micro-membranes because wrinkles are mechanically weak parts decreasing failure strength of graphene micro-membranes.³³ Accordingly, many efforts have been devoted to the preparation of wrinkle-free graphene, including the hot pressing of the metal substrates, introducing an adhesion layer, wedging transfer, double-transfer procedure, and so forth. However, most of previous methods require complicated and rigorous procedures, and the results also need to be more improved because the amount of the wrinkles still cannot be ignored. For these reasons, it is challenging to develop an efficient and facile strategy for wrinkle-free graphene with high-quality.

3.2. PMMA-mediated transfer

When graphene prepared by CVD is transferred onto a target substrate, PMMA has been particularly widely used as a protective layer, furnishing mechanical strength and easy of handling. The overall procedure for transferring graphene *via* the conventional wet-transfer is depicted in figure 3-1. A solution of 4.5 wt% PMMA dissolved in anisole (PMMA, 950 A9, MicroChem) was prepared by stirring for 1h at room temperature. The PMMA layer was spin-coated onto the as-grown graphene/Cu stack at 2500rpm for 60s followed by baking for 15min in a convection oven at 80°C in order to evaporate residual solvents and make conformal contact between PMMA and graphene. The thickness of PMMA layer was ~ 320 nm measured by surface profilometer (see figure 3-5 (b) and table 2). The back-side graphene was eliminated by oxygen plasma for 3min at a plasma power of 100 W. This is because the entire surface of Cu foil was covered with graphene during the CVD growth process, and the back-side graphene could be broken and floated in the etching solution unless it was removed. Afterwards, The Cu foil underneath the graphene was etched out by copper etchant (also referred to as iron(III) chloride (FeCl₃) aqueous solution, CE-100, Transene Company Inc.) for 15min. The floated PMMA/graphene stack on the surface of the etchant was transferred to a DI water bath to be rinsed multiple times. In a subsequent step, it was moved to a 10wt% hydrochloric acid (HCl) (ACS grade, Hydrochloric Acid 36.5~38%, VWR Analytical) solution to remove the etchant residue in the form of metallic salt, on the graphene film. The PMMA/graphene film was rinsed with distilled water several times to remove the HCl

residue. Once the rinsing process was done, the PMMA/graphene film was scooped out onto SiO₂(300nm)/Si wafer at room temperature and compressed N₂ gas was gently blown on the PMMA/graphene/SiO₂/Si sample to eliminate water molecules between the PMMA/graphene film and the wafer. After the drying step by N₂, the sample was placed in a convection oven held at 80°C for 1 hour to thermally evaporate the moisture at the interface leading a good adhesion of graphene on the substrate. Finally, the PMMA was removed from the graphene/SiO₂/Si wafer by placing the sample into an acetone solvent bath. The graphene sample was washed with isopropyl alcohol and then was blow dried again using high purity N₂ at room temperature.

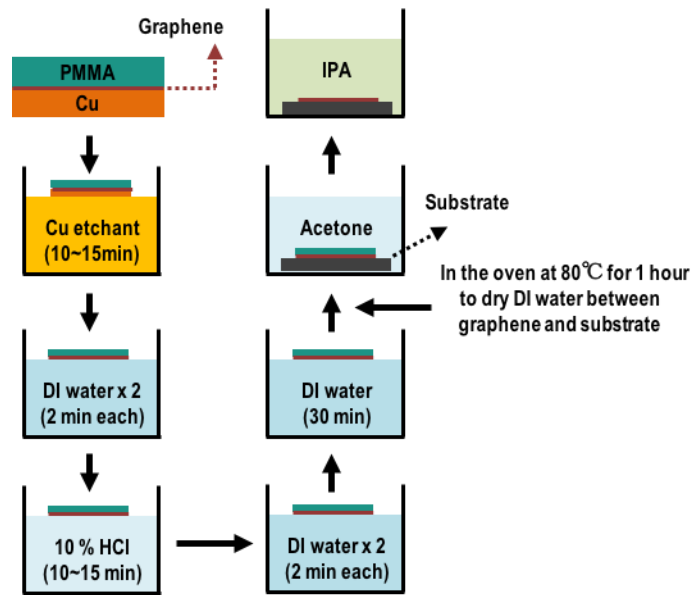


Figure 3-1. An overall process for transferring CVD-grown graphene by PMMA-mediated transfer, also referred to as the conventional wet transfer.

3.2.1. Limitation of the conventional transfer method

Although the PMMA-mediated transfer method is the most common one to transfer CVD-grown 2D materials including graphene, there are always residues left on graphene and there is a weak p-doping effect on graphene.³⁴ The insulating polymer residues act as scattering centers thus inhibit charge carrier transport and degrade performance of electronic devices.³⁵

Furthermore, as it mentioned above, the as-transferred graphene on a flat target substrate usually exhibits many wrinkles due to the differences between the CTE of graphene and that of Cu foil. These wrinkles were still present after the graphene is transferred to the target substrate, as

illustrated in Figure 3-2 (a). Corresponding optical microscope (OM) and atomic force microscope (AFM) images of transferred graphene on a 300 nm SiO₂/Si substrates show clear evidence of wrinkles on the areas covered with as-transferred graphene by PMMA (Figure 3-2 (b)-(c)).

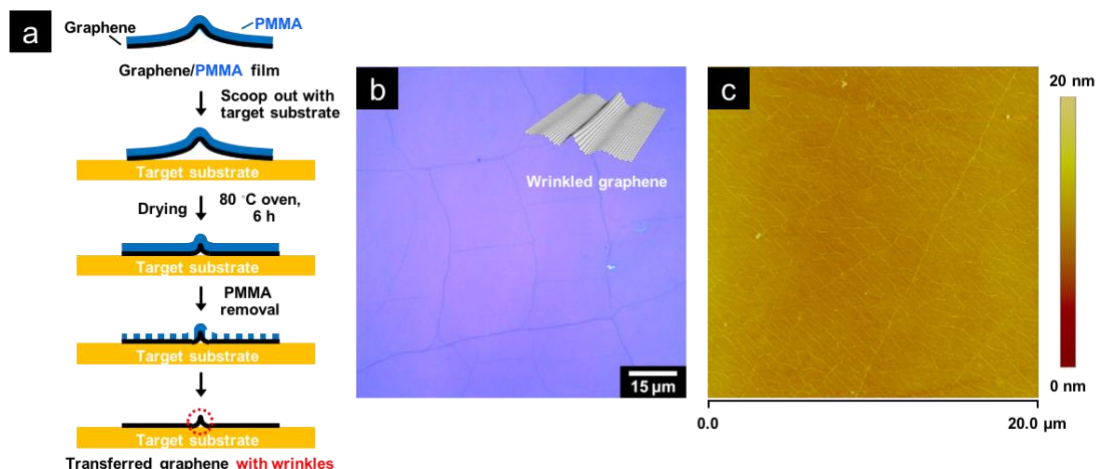


Figure 3-2. (a) Schematic illustration of the PMMA-supported graphene transfer procedure onto a target substrate, representing the sequential steps after etching Cu foil. (b) OM image and (c) AFM image of transferred graphene film onto SiO₂/Si substrate which is corresponding to the last schematic in (a).

3.3. PDMS/PMMA double-layer transfer

Here, we present a novel method of transferring CVD-grown 2D materials to remove the wrinkles in graphene. Figure 3-3 illustrates sequential steps of our double-layer transfer technique in detail. The preparation of PMMA layer was the same as aforementioned PMMA-mediated transfer technique. A solution of 50 wt% PDMS (Sylgard 184, Dow Corning) in hexane was prepared by mixing an elastomer and a curing agent with the ratio of 5:1 and diluting it with hexane. The PDMS solution spun onto the top of PMMA layer at 2500rpm for 60sec and thermally cured for 60min in an oven at 80°C. After the crosslinking process, the overall processes were the same as the PMMA-mediated transfer method except for the final step before placing PDMS/PMMA/graphene stack onto the target substrate. A hot water bath was used to thermally expand the PDMS layer. The PDMS/PMMA/graphene stack on the surface of DI water was maintained at 80°C for 1h. Thereafter, the PDMS/PMMA/graphene film was transferred on SiO₂ (300nm)/Si substrate which was followed by drying in an oven at 80°C for 1 hour to evaporate the

water molecules from the interface completely, allowing the PDMS/PMMA/graphene stack be fully in contact with the wafer. At last, the PDMS/PMMA double-layer was removed by immersing the sample in acetone bath and then the sample was rinsed with isopropyl alcohol (IPA).

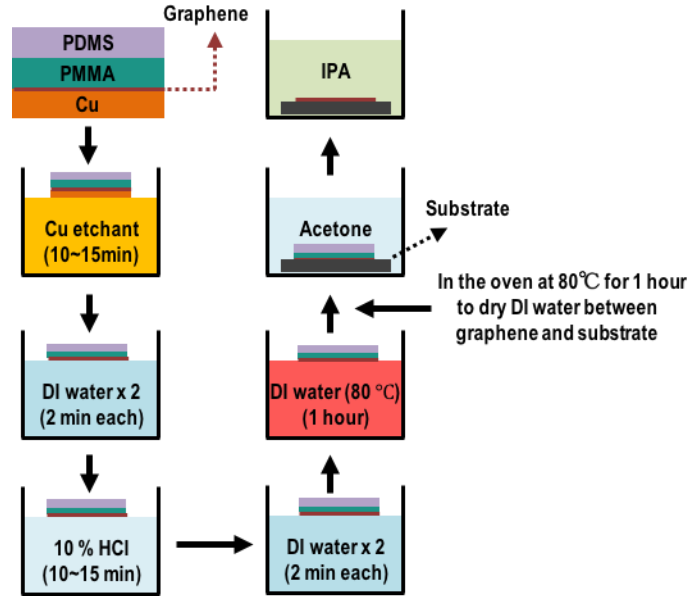


Figure 3-3. Schematic images of our PDMS/PMMA double-layer transfer method to transfer CVD-grown graphene onto desirable substrates.

3.3.1. Mechanism of the double-layer transfer method

The schematic illustrations in Figure 3-4 (a) depict the scenarios for the new graphene transfer method. Basically, PMMA is spin-coated on a graphene/Cu foil with the thickness of ~ 320 nm. For the new approach, however, the PDMS layer has a thickness of ~ 10 μm , which we call the 'expandable layer', was additionally introduced to the PMMA/graphene film to remove the wrinkles by introducing thermally induced tensile stress on the graphene (Figure 3-5 (a)). In figure 3-5 (b) and table 2, the thickness of PMMA, PDMS, and PDMS/PMMA thin film was measured by surface profilometer. Figure 3-4 (b)-(c) shows the optical microscope image and AFM image of the transferred graphene film onto SiO_2/Si substrate.

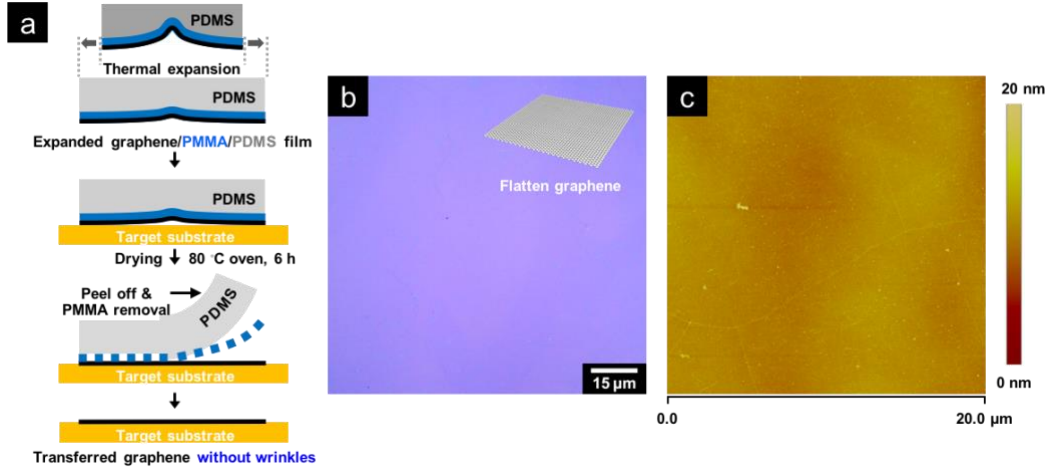


Figure 3-4. (a) Schematically illustrated our optimal PMMA/PDMS double layer transfer process onto a target substrate, for CVD grown-2D materials which is following the etching of Cu substrate. Corresponding (b) OM image and (c) AFM image of transferred graphene film onto SiO₂/Si substrate.

In contrast to the conventional wet-transfer method, the PDMS/PMMA/graphene stack is placed onto a moderately hot DI water maintained at 80 °C for 1 h before scooping out. It is worth to note that the PDMS is a rubbery polymer exhibiting high CTE value of $310 \times 10^{-6} \text{ K}^{-1}$ and the cross-linked PDMS film exhibits good thermal-mechanical stability even at high temperature. Considering that the CTE value of the PDMS is much higher than those of polymeric supporting materials previously used for graphene transfer, the PDMS layer is isotropically expanded with applied thermal energy in the hot DI water bath. An increased length (l) at a given increased temperature (ΔT) may be expressed as, $l_0 \{1 + (310 \times 10^{-6} \text{ K}^{-1}) \Delta T\}$. The isotropic expansion of the PDMS layer allowed the PDMS/PMMA/graphene film to become more flattened and tightly attached to the final substrate. As a result, it can be expected that the graphene wrinkles which originated from the CTE mismatching could be diminished and/or eliminated by the stretched PDMS layer, whereas these wrinkles would still have remained using the conventional PMMA-mediated transfer method as shown in the upper-right side illustration of figure 3-5 (a).

Since the PMMA layer also have an important part in the new graphene transfer procedure, the roles of the PMMA layer acting as a 'gluing layer' need to be addressed. The PMMA layer served to avoid contamination of graphene. Furthermore, the PMMA layer is able to dissolve in widely used organic solvent that allows to remove the crosslinked PDMS layer which is not soluble as a sacrificial layer. By being placed between the PDMS layer and the graphene sheet, the PMMA

layer protects the graphene from contamination by the low-molecular weight siloxane oligomers present in the PDMS layer. Moreover, the PMMA layer has a relatively high work of adhesion ($W_{\text{PMMA-Graphene}}$) with the graphene that is larger than that between the graphene and the PDMS layer ($W_{\text{PDMS-Graphene}}$). In general, the PDMS has lower surface energy than most organic polymers. That is, it is difficult for chemical species to interact with the surface, and adhesion is poor. The work of adhesion between two materials can be obtained by the Young-Dupré equation: $W_{12} = \gamma_1 + \gamma_2 - \gamma_{12}$, where γ_1 and γ_2 are the surface energies of the two new surfaces, and γ_{12} is the interfacial tension, which is defined as, $\gamma_{12} = \gamma_1 + \gamma_2 - 2(\gamma_1 \cdot \gamma_2)^{0.5}$. In these calculations, we used $\gamma = 20 \text{ mJ m}^{-2}$ for PDMS, 38 mJ m^{-2} for PMMA and 62 mJ m^{-2} for graphene (based on the value for highly ordered pyrolytic graphite(HOPG)). Because $\gamma_{\text{PMMA}} > \gamma_{\text{PDMS}}$, the interaction between the graphene and the PMMA layer can be expected to be stronger. The $W_{\text{PMMA-Graphene}}$ value is estimated to be 97.1 mJ m^{-2} , ~ 1.4 times greater than the $W_{\text{PDMS-Graphene}}$. The relatively high γ_{PMMA} value leads to good adhesion with the graphene, rather than the PDMS-graphene or PMMA-PDMS contact. (bottom-right side of figure 3-5 (a))

Consequently, a clean and continuous transferred graphene surface is observed in the corresponding OM and AFM images (figure 3-2 (b)-(c) for PMMA-mediated transfer and figure 3-4 (b)-(c) for double-layer transfer). It suggests that the graphene transferred by the PDMS/PMMA double layered transfer method has a much more uniform morphology with significantly fewer wrinkles than the graphene transferred by the conventional PMMA-mediated transfer method.

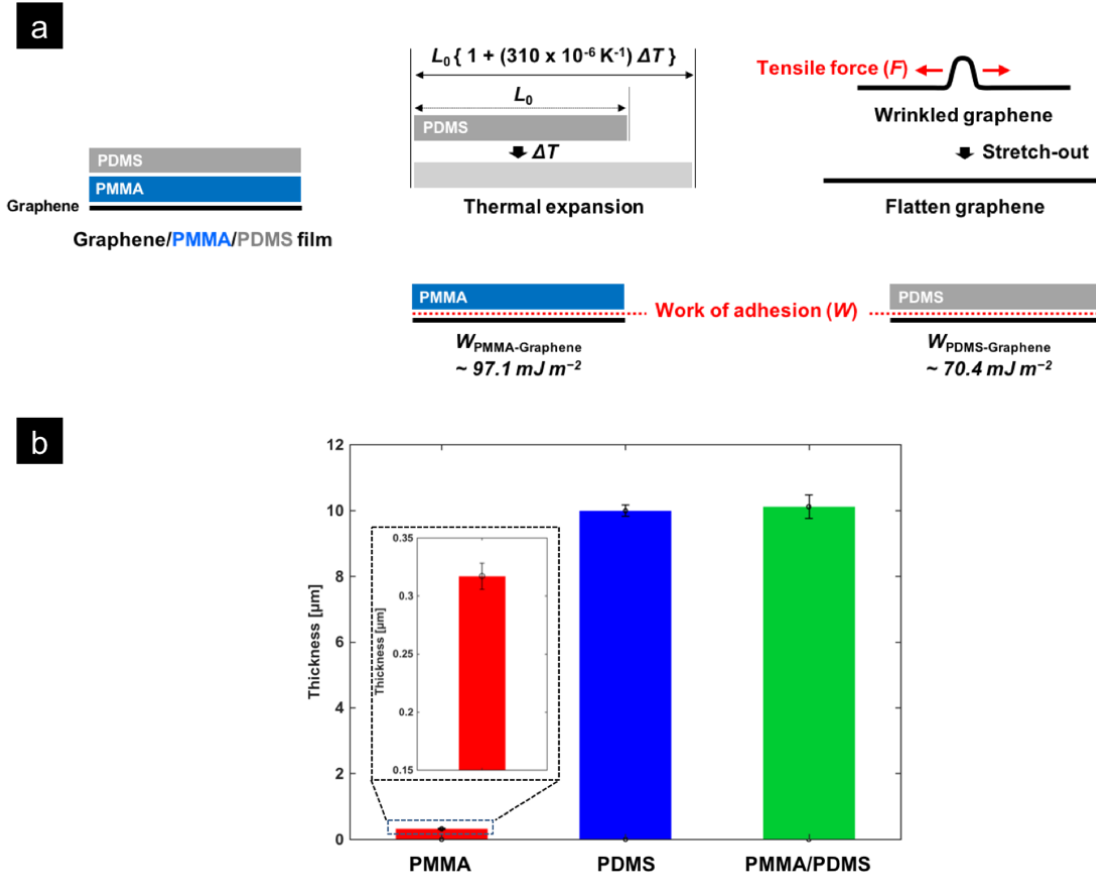


Figure 3-5. (a) (left) Cross-sectional image of the PDMS/PMMA/graphene film. The PDMS and PMMA layers play a role of an expandable and a gluing layer, respectively. Illustration of two possible reasons to reduce wrinkles in graphene, tensile stain aspect in upper-right side and adhesion energy aspect in bottom-right side. Note that interfacial tension (γ) values of PDMS, PMMA and graphene are 20, 38 and 62 mJ m^{-2} , respectively. (b) Comparison of film thickness of PMMA, PDMS and PDMS/PMMA double-layer.

	Average Thickness (μm)	Standard Deviation (μm)	With 95% Confidential Level (μm)
PMMA	0.317	0.0112	[0.301:0.333]
PDMS	9.985	0.169	[9.750:10.219]
PMMA/PDMS	10.106	0.361	[9.606:10.605]

Table 2. Results of film thickness measured by a surface profiler.

3.3.2. Quantitative analysis of wrinkles in graphene

Figure 3-6 (a)-(b) are the AFM images of a graphene samples on SiO₂/Si transferred by the conventional PMMA-mediated and the PMMA/PDMS double layered transfer methods. In the conventionally transferred graphene sample, a large number of graphene wrinkles can be clearly observed. In contrast, for the graphene transferred by the PMMA/PDMS double layered method, there is a significant decrease in both the number and the height of the graphene wrinkles.

To further clarify the findings obtained from the AFM measurement, quantitative wrinkle analysis was performed with three different selected regions (red, blue, and black boxes in figure 3-6 (a)-(b)). The wrinkle height and width could be extracted from the height profiles, and the wrinkle density was calculated by counting the number of wrinkles in 400 μm² of the graphene surface. Figure 3-6 (c)-(d) depicts the distribution of the both height and width of graphene wrinkles (total ~30 samples). Compared with the graphene samples transferred by the PMMA, the graphene samples transferred by the PDMS/PMMA double layer method exhibit smaller wrinkle heights and width with a narrower distribution. The Gaussian distributions indicate that the average wrinkle height and width were estimated as 1.5 ± 0.4 nm and 36.4 ± 5.3 nm for the graphene samples transferred by the PMMA/PDMS double layered method, which is relatively lower than those of graphene samples transferred by the conventional PMMA-mediated method (height: 4.5 ± 0.7 nm, width: 53.4 ± 7.5 nm).

Furthermore, Figure 3-6 (e) summarizes the results for the number of wrinkles counted. The average wrinkle densities were 1.31 ± 0.21 ea/μm² and 0.02 ± 0.01 ea/μm² for the graphene transferred by the PMMA-mediated and the PMMA/PDMS double layered method, respectively. It should be noted that the approximately one-sixty fifth lower wrinkle density value of the graphene transferred by the new method implies a tremendously flatter surface in comparison with the graphene transferred by the conventional method.

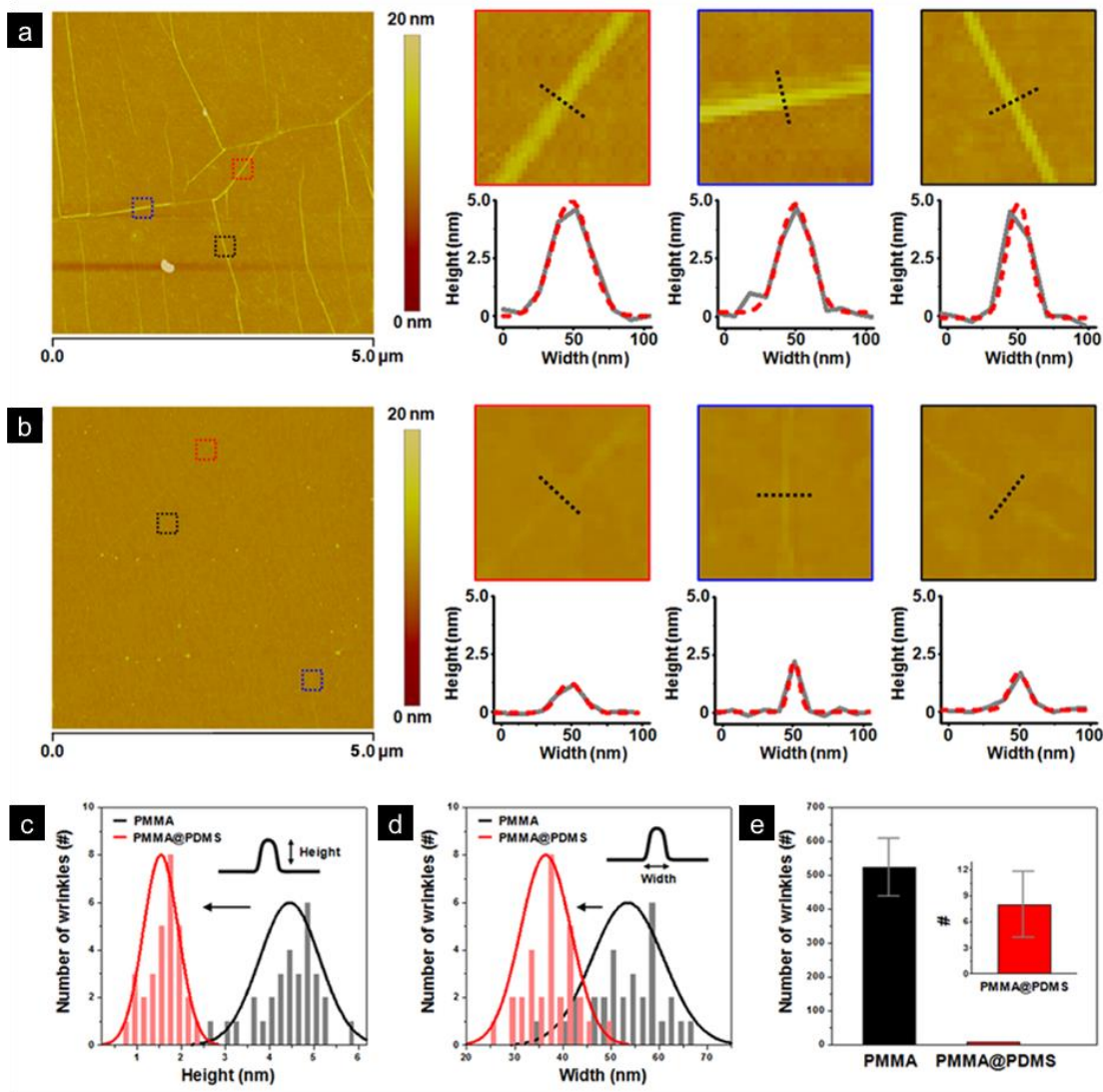


Figure 3-6. The AFM images of graphene transferred to a 300 nm SiO₂/Si substrate by using (a) the conventional PMMA-mediated and (b) the PDMS/PMMA double-layer transfer method. The corresponding AFM images and height profiles were taken with three different selected regions (red, blue, and black boxes). The wrinkle (c) height and (d) width distribution of graphene samples transferred by the conventional PMMA-mediated (black) and the PDMS/PMMA double-layer (red) transfer method. (e) Histograms of wrinkle density for the conventional PMMA-mediated (black) and the PDMS/PMMA double-layer (red) transfer method. The wrinkles in 400 μm² of graphene surface are counted. The indicated error bars of measurements are shown.

3.4. Wax-supported transfer

Apart from the wrinkle formation, another issue with using conventional PMMA-mediated graphene transfer method is the PMMA residues being left on the graphene surface as mentioned in 3.2.1. It has been reported that the PMMA cannot be completely removed with solvents and inevitably remained PMMA residues adversely affecting the graphene's intrinsic electrical properties. Thermal annealing has been regarded as an effective post-step to remove PMMA residues on graphene film. However, the cleanliness of graphene surface still remains unsatisfactory and the high annealing temperature increases coupling between graphene and SiO₂ layer, leading to heavy hole-doping and decrease in mobility.

In this respect, we suggest a novel transfer technique to mitigate wrinkles and reduce the density of residues simultaneously. We have found that paraffin wax, simple hydrocarbons (C_nH_{2n+2} where $20 < n < 40$), is very efficient to be used as a support layer. Different from previous double-layer (PDMS/PMMA), it is simply one layer, strong enough to support graphene without damages and it can be easily eliminated from graphene thin film because it dissolves in universal organic solvent such as xylene (known as the best solvent to dissolve paraffin wax). Besides, it has a weak interaction with graphene and a comparable value of CTE ($200\sim 350 \times 10^{-6} K^{-1}$) with one of PDMS ($310 \times 10^{-6} K^{-1}$) as indicated in table 3. All of these enable damage-free transfer with minimized wrinkles and residues.



Properties	PMMA	Wax (paraffin)
Structure	 (C ₅ O ₂ H ₈) _n	 C _n H _{2n+2} (20 < n < 40)
Density (g cm ⁻³)	1.17	0.8-0.9
Melting temperature (°C)	160	57.2
Coefficients of Thermal Expansion (x10 ⁻⁶ K ⁻¹)	70	200~350
Thermal conductivity (W mK ⁻¹)	0.19	0.15-0.21
Young's modulus (Mpa)	1800 - 3100	61~275 (Solid state) 0.1 (Liquid state)
Solubility parameter (MPa ^{1/2}) Polymer/Solvent	19/19.7 (PMMA/Acetone)	16.6 - 16.9/16.8 (wax/Cyclohexane)

Table 3. Comparison for chemical, physical and mechanical properties of PMMA and paraffin wax.

Figure 3-7 illustrates the overall procedures of our wax-transfer technique. Firstly, a thin layer of wax which dissolved in xylene with a concentration of 50wt% was spin-coated on the CVD-grown graphene film at 1000rpm for 2min and was dried at room temperature. Apart from the hot-water bath and the drying step, all other procedure was the same as those in the double-layer transfer method. In this case, the wax/graphene stack on the DI water bath was heated up to 50°C instead of 80°C for the same amount of time. The reason of the lower temperature is that the wax which we used has melting point in the range of 45~65°C confirmed by the DSC thermal analysis (figure 3-8). Afterwards, as the final step of the transfer, the wax on graphene was removed by soaking the sample in xylene and followed by rinsing the sample with IPA.

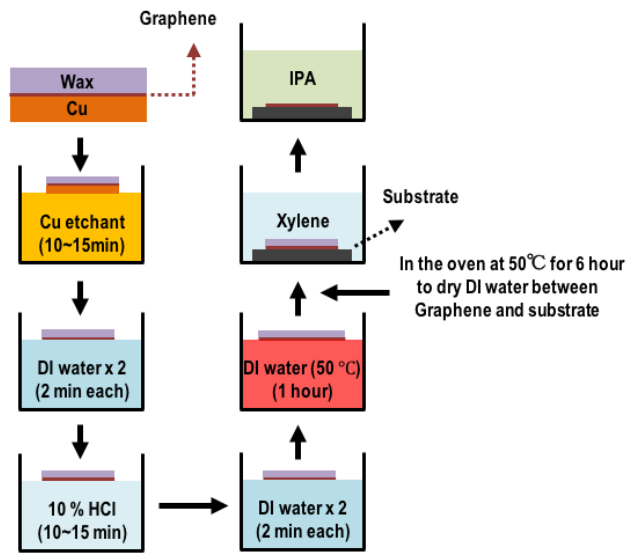


Figure 3-7. Schematic process flow of wax-supported transfer method for CVD-grown monolayer graphene.

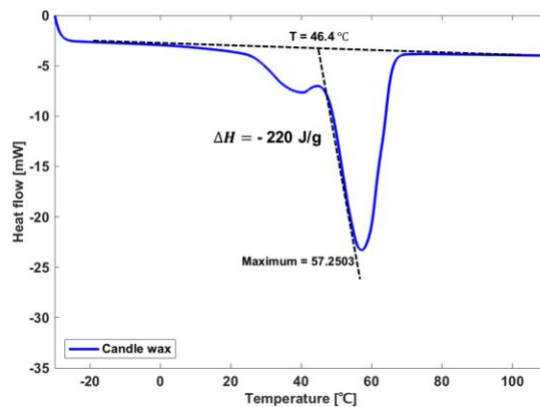


Figure 3-8. Differential Scanning Calorimetry (DSC) thermal analysis of paraffin-wax which was used in our experiments, displaying thermal transition of the polymer.

The investigation of the top surface of monolayer graphene was carried out via OM and SEM. For comparison, we investigated surface properties of both PMMA-transferred and wax-transferred graphene film. Figure 3-9 shows the OM and SEM images of the graphene surface on SiO₂/Si which was transferred by the PMMA-mediated transfer method ((a) and (c)) and our wax-supported transfer technique ((b) and (d)), respectively. The CVD-grown graphene is mostly single layer with randomly distributed bilayer islands on its surface. A large number of wrinkles, polymer residues and broken region were clearly observed on the continuous graphene film transferred by PMMA under both OM and SEM as shown in figure 3-9 (a) and (c). In contrast, the density of wrinkles shows a clear reduction and the wax-transferred graphene film is much cleaner. The wax residues were barely observed even under SEM (figure 3-9 (b) and (d)).

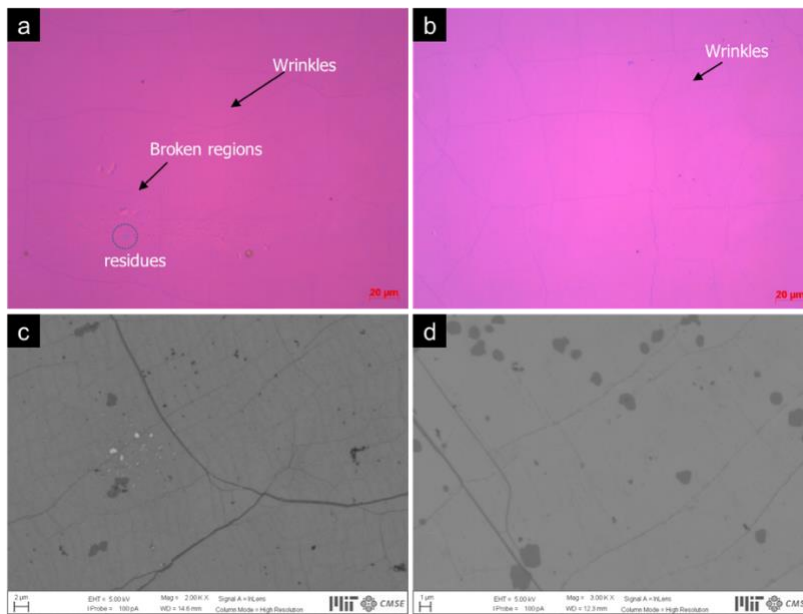


Figure 3-9. OM/SEM images of monolayer graphene on SiO₂(300nm)/Si wafer which was transferred via (a)/(c) the conventional wet transfer method and (b)/(d) our wax-supported transfer method, respectively.

3.4.1. Mechanism of wax-mediated transfer method

The basic concept to flatten out the wrinkles in graphene thin layer is the same as the previous double-layer method. In these transfer method, we exploit the thermal properties of the polymeric support materials. Here, the paraffin wax layer acts as the expandable layer with high

CTE value range of $200\sim 350 \times 10^{-6} \text{ K}^{-1}$. It isotropically expands upon heating and contract during cooling. If it is a linear solid, the change in length with temperature obeys the linear thermal expansion rule as can be expressed, $l_f = l_0 \{1 + \alpha (T_f - T_0)\}$ where l_0 and T_0 are the initial length and temperature, l_f and T_f are the final length and temperature and α is the linear thermal expansion coefficient, respectively (figure 3-10 (a)). Therefore, wax with very high TCE applies mechanical tensile strain to thin graphene layer underneath it when heated up, which helps to smooth out the wrinkles in the graphene. As shown in figure 3-9 (d), it is found that applied tensile strains are effective to eliminate small wrinkles rather than the large ones.

We also used AFM to characterize the surface of PMMA-transferred and wax-transferred graphene films for a comparison. AFM images in figure 3-10 (b) and (d) show a large number of wrinkles along the whole graphene film. On the contrary, wrinkles in wax transferred graphene film are not so noticeable (figure 3-10 (c) and (e)). The density of wrinkles and residues was calculated by color contrast arising from height difference in the AFM images, which demonstrated that the density of them was decreased by 63% when used wax-mediated transfer method.

In contrast to the conventional wet-transfer method, wax-transferred graphene films have less residues that can be explained by solubility of support polymer and adhesion between support polymer and graphene film. As stated earlier, the structure of paraffin is a simple hydrocarbon chain so that wax is freely soluble in universal organic solvent such as xylene according to the rule of “like dissolves like”. Furthermore, the work of adhesion was studied to compare interaction between the carrier material and the graphene film. Here we used $\gamma = 41 \text{ mJ m}^{-2}$ for PMMA³⁶, 35 mJ m^{-2} for paraffin wax³⁷ and 62 mJ m^{-2} for graphene (based on the value for highly ordered pyrolytic graphite(HOPG)) in order to calculate the work of adhesion (W_{12}) by the Young-Dupré equation which can be expressed as $W_{12} = \gamma_1 + \gamma_2 - \gamma_{12} = 2(\gamma_1 \cdot \gamma_2)^{1/2}$, where γ_1 and γ_2 are the surface energies of the two new surfaces, and γ_{12} is the interfacial tension ($\gamma_{12} = \gamma_1 + \gamma_2 - 2(\gamma_1 \cdot \gamma_2)^{1/2}$). Note that the surface of polymer was directly measured from polymer melt and extrapolated to 20°C. From the calculation, $W_{\text{PMMA-Graphene}}$ ($\sim 101 \text{ mJ m}^{-2}$) was about 1.1 times larger than $W_{\text{wax-Graphene}}$ ($\sim 93 \text{ mJ m}^{-2}$). It might reasonably support the phenomena of less residues in the case of wax transferred graphene compare to the number of PMMA residues in PMMA-transferred graphene. As a result, it proposes that the wax transferred graphene represents cleaner and continuous film with less residues, wrinkles and broken region when compared to PMMA-transferred graphene.

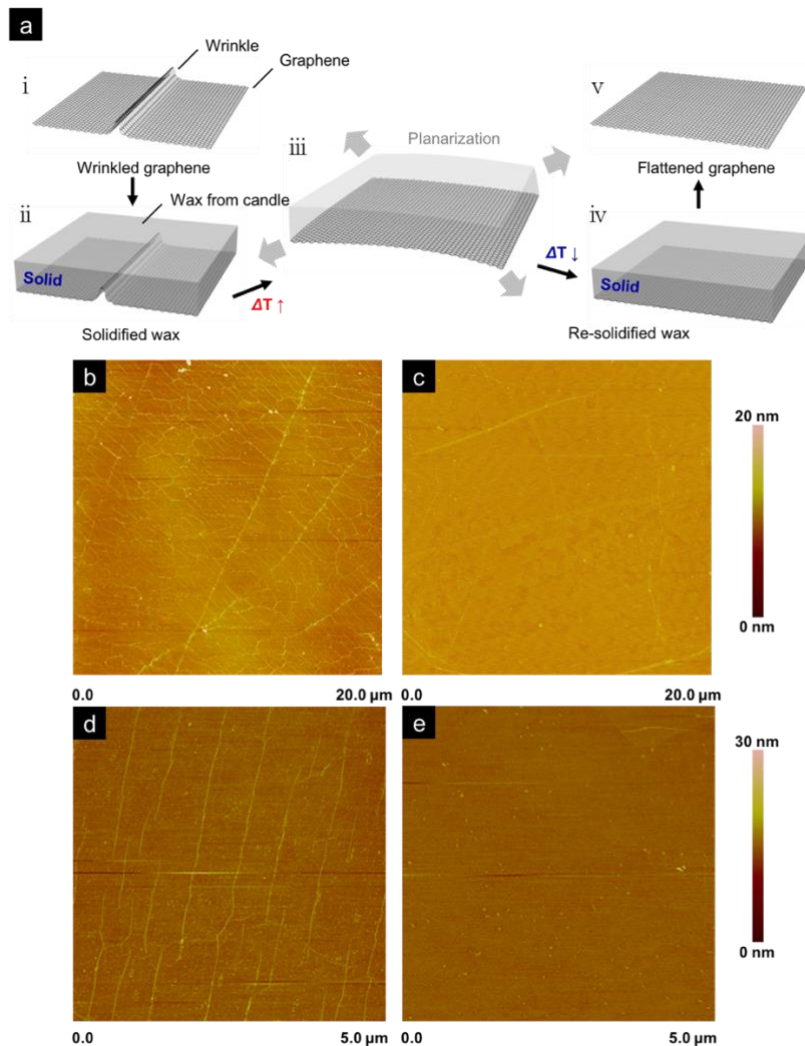


Figure 3-10. (a) Schematic illustration to describe the mechanism of our wax-mediated transfer method. Low magnification AFM height images of graphene film transferred by using (b) PMMA and (c) paraffin-wax. Corresponding high magnification AFM images of graphene by (d) PMMA-mediated transfer process and (e) wax-supported transfer process.

3.4.2. Dependence of thermal expansion effect of wax on temperature

Since wax has a broad melting point range of 45~65 °C, the temperature dependence of thermal expansion effect of the wax layer was investigated by characterizing the surface of wax-transferred graphene at each temperature using AFM. We have tried to change the temperature in hot-water bath process to control the thermal strain. In figure 3-11 (a) and (b), the thermal expansion effect of wax was not effective at low temperature due to the small difference in temperature. At high temperatures which was higher than melting temperature, as the wax become

liquid like, the strain from thermal expansion cannot be transferred to graphene effectively. In addition, more tears in the graphene film were observed (figure 3-11 (e) and (f)). We found that the optimal temperature to minimize wrinkles by applying tensile force to graphene film was 50°C.

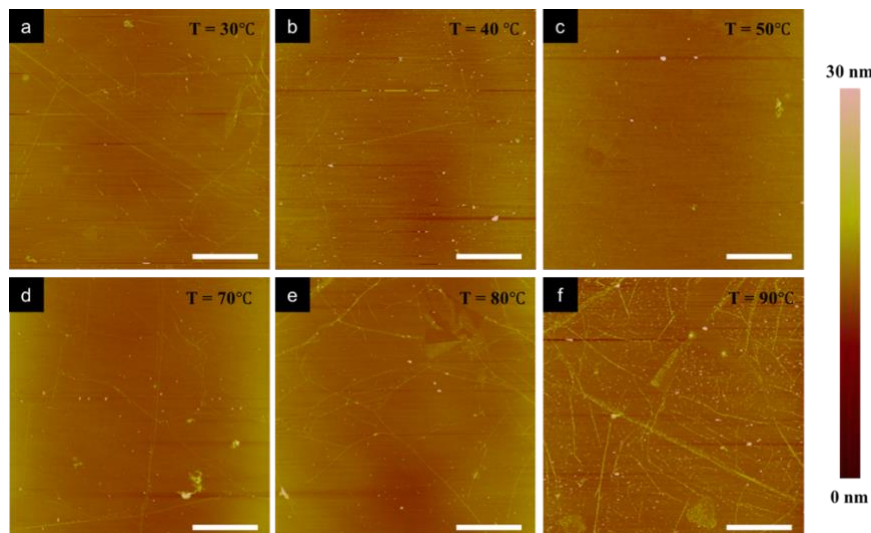


Figure 3-11. The thermal expansion effects of paraffin-wax on monolayer graphene film with respect to temperature. The scale bars in (a)-(f) are all 5 μm .

3.4.3. Improvement in surface quality

Figure 3-12 (a)-(b) are the AFM images of the PMMA-transferred and the wax-transferred monolayer graphene sample on SiO_2/Si , respectively. The surface quality of graphene transferred by our wax-transfer method was much cleaner with minimized wrinkles and residues in comparison to graphene surface transferred by the conventional PMMA transfer method.

As we analyzed the wrinkles via AFM above, the quantitative wrinkle analysis was performed with three different selected regions (red, blue, and black boxes in figure 3-12 (a)-(b)). The wrinkle height and width could be extracted from the height profiles, and the wrinkle density was calculated by counting the number of wrinkles in $400 \mu\text{m}^2$ of graphene surface. Figure 3-12 (c)-(d) represent the distribution of the both height and width of graphene wrinkles in total ~ 30 samples. Compared with conventional PMMA transfer method, the wax-transferred graphene samples display smaller wrinkle heights and narrower wrinkle width. The Gaussian distributions indicate that the average wrinkle height and width were estimated as $4.8 \pm 0.8 \text{ nm}$ and $53.9 \pm 7.5 \text{ nm}$ for PMMA-transferred graphene samples, which is relatively larger than those of graphene

samples transferred by our wax transfer technique which has 1.1 ± 0.4 nm for wrinkle height and 37.1 ± 6.9 nm for wrinkle width. In summary, figure 3-12 (e) summarizes the results for the number of wrinkles counted. The average wrinkle densities were significantly reduced from 1.28 ± 0.21 ea/ μm^2 to 0.015 ± 0.01 ea/ μm^2 when transferred by the wax-mediated transfer method.

Figure 3-12 (a)-(b) are the AFM images of the PMMA-transferred and the wax-transferred monolayer graphene sample on SiO₂/Si, respectively. The surface quality of graphene transferred by our wax-transfer method was way cleaner with minimized wrinkles and residues in comparison to graphene surface transferred by the conventional wet transfer method.

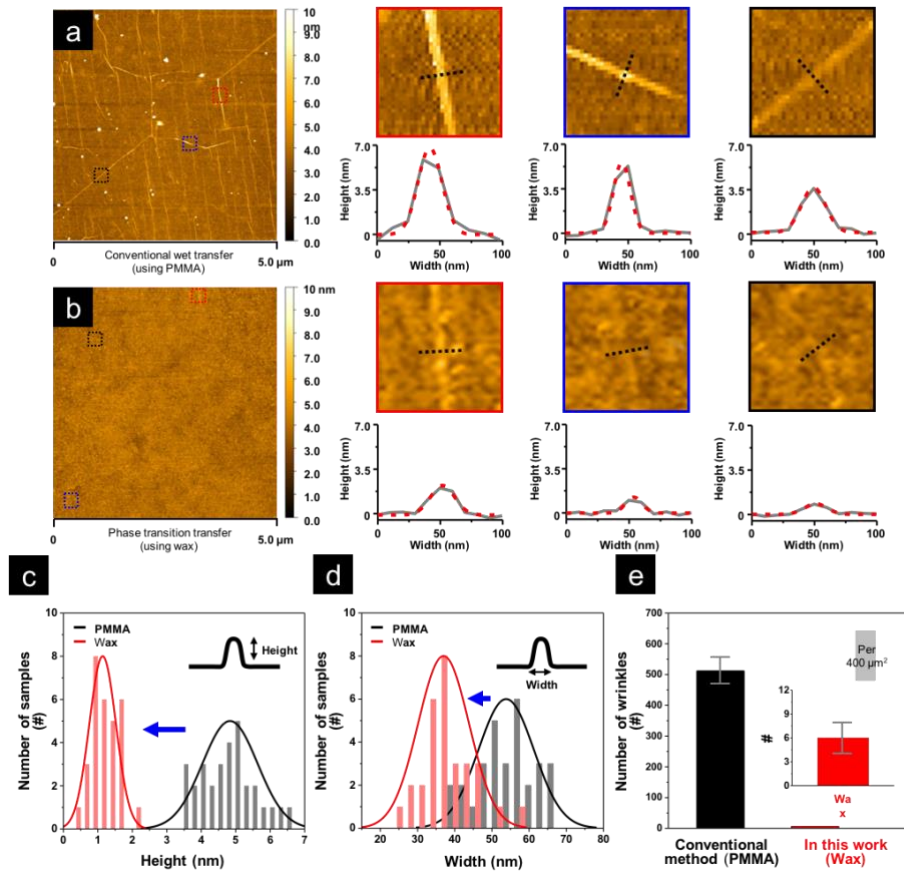


Figure 3-12. The AFM images of graphene transferred to a 300 nm SiO₂/Si substrate by using (a) the conventional PMMA-mediated and (b) the wax-mediated transfer methods. The corresponding AFM images and height profiles were taken with three different selected regions (red, blue, and black boxes). The wrinkle (c) height and (d) width distribution of graphene samples transferred by the conventional PMMA-mediated (black) and the wax-mediated (red) transfer methods. (e) Histograms of wrinkle density for the conventional PMMA-mediated (black) and wax (red) transfer method. The wrinkles in 400 μm^2 of graphene surface are counted. The indicated error bars of measurements are shown.

Chapter 4.

Conclusions

In this thesis, we have used chemical vapor deposition to synthesize high-quality continuous monolayer graphene and few-layer graphene films on Cu foil. These CVD-grown graphene films were characterized by OM, AFM, SEM and Raman spectroscopy. It was found that the mono- and few-layer graphene were continuous over large area. In addition, the as-grown monolayer graphene film presents high ratio of Raman peak intensities (I_{2D}/I_G) and sharp 2D band. In terms of electrical properties, the single-layer graphene exhibits Hall mobility reaching $\sim 2200 \text{ cm}^2 \text{ V}^{-1} \text{ s}^{-1}$ and R_s of $480 \text{ } \Omega/\text{sq}$ which are quite reasonable values in a CVD-grown un-doped polycrystalline monolayer graphene films.

In the following, we have developed two novel methods to transfer as-grown graphene onto target substrates. Firstly, a common acrylic polymer PMMA and a rubbery PDMS were used to transfer as a double-layer. The wrinkles in graphene were quantitatively evaluated. It has been found that high quality of an as-transferred graphene is obtained *via* the double layered method, which shows not only less wrinkles density of $0.02 \pm 0.01 \text{ ea}/\mu\text{m}^2$ but also smaller height and width of $1.5 \pm 0.4 \text{ nm}$ and $36.4 \pm 5.3 \text{ nm}$ respectively. Furthermore, paraffin wax was exploited as a support layer. Different from previous double-layer (PDMS/PMMA), it is simply one layer, strong enough to support graphene without damages and it can be easily eliminated from graphene thin film due to freely soluble in organic solvents. Besides, a weak interaction with graphene and a comparable value of CTE ($200\sim 350 \times 10^{-6} \text{ K}^{-1}$) with one of PDMS ($310 \times 10^{-6} \text{ K}^{-1}$) enable damage-free transfer with minimized wrinkles and residues. In the quantitative viewpoints, the average wrinkle densities were significantly reduced from $1.28 \pm 0.21 \text{ ea}/\mu\text{m}^2$ to $0.015 \pm 0.01 \text{ ea}/\mu\text{m}^2$ when transferred by the wax-mediated transfer method. These high-quality monolayer graphene with minimum wrinkles and residues would be the best promising candidate for electronics, sensors and membrane.

References

- (1) Novoselov, K. S.; Geim, A. K.; Morozov, S. V.; Jiang, D.; Zhang, Y.; Dubonos, S. V.; Grigorieva, I. V.; Firsov, A. A. Electric Field Effect in Atomically Thin Carbon Films. *Science* (80-.). **2004**, *306*, 666–669.
- (2) Bolotin, K. I.; Sikes, K. J.; Jiang, Z.; Klima, M.; Fudenberg, G.; Hone, J.; Kim, P.; Stormer, H. L. Ultrahigh Electron Mobility in Suspended Graphene. *Solid State Commun.* **2008**, *146*, 351–355.
- (3) Jiang, Z.; Zhang, Y.; Stormer, H. L.; Kim, P. Quantum Hall States near the Charge-Neutral Dirac Point in Graphene. *Phys. Rev. Lett.* **2007**, *106802*, 1–4.
- (4) Du, X.; Skachko, I.; Duerr, F.; Luican, A.; Andrei, E. Y. Fractional Quantum Hall Effect and Insulating Phase of Dirac Electrons in Graphene. *Nature* **2009**, *462*, 10–13.
- (5) Novoselov, K. S.; MaCann, E.; Morozov, S. V.; Fal’ko, V. I.; Katsnelson, M. I.; Zeitler, U.; Jiang, D.; Schedin, F.; Geim, A. K. Unconventional Quantum Hall Effect and Berry’s Phase of 2π in Bilayer Graphene. *Nat. Phys.* **2006**, *2*, 177–180.
- (6) Nair, R. R.; Blake, P.; Grigorenko, A. N.; Novoselov, K. S.; Booth, T. J.; Stauber, T.; Peres, N. M. R.; Geim, A. K. Fine Structure Constant Defines Visual Transparency of Graphene. *Science* (80-.). **2008**, *320*, 1308.
- (7) El-Kady, M. F.; Strong, V.; Dubin, S.; Kaner, R. B. Laser Scribing of High-Performance and Flexible Graphene-Based Electrochemical Capacitors. *Science* (80-.). **2012**, *335*, 1326 LP-1330.
- (8) Kim, K. S.; Zhao, Y.; Jang, H.; Lee, S. Y.; Kim, J. M.; Kim, K. S.; Ahn, J.-H.; Kim, P.; Choi, J.-Y.; Hong, B. H. Large-Scale Pattern Growth of Graphene Films for Stretchable Transparent Electrodes. *Nature* **2009**, *457*, 706–710.
- (9) Lin, Y. M.; Dimitrakopoulos, C.; Jenkins, K. A.; Farmer, D. B.; Chiu, H. Y.; Grill, A.; Avouris, P. 100-GHz Transistors from Wafer-Scale Epitaxial Graphene. *Science*, 2010, *327*, 662.
- (10) Schedin, F.; Geim, A. K.; Morozov, S. V.; Hill, E. W.; Blake, P.; Katsnelson, M. I.; Novoselov, K. S. Detection of Individual Gas Molecules Adsorbed on Graphene. *Nat. Mater.* **2007**, *6*, 6–9.
- (11) Heer, W. A. De; Berger, C.; Wu, X.; First, P. N.; Conrad, E. H.; Li, X.; Li, T.; Sprinkle, M.; Hass, J.; Sadowski, M. L.; *et al.* Epitaxial Graphene. *Solid State Commun.* **2007**, *143*, 92–100.
- (12) Mattevi, B. C.; Eda, G.; Agnoli, S.; Miller, S.; Mkhoyan, K. A.; Celik, O.; Mastrogiovanni, D.; Granozzi, G.; Garfunkel, E.; Chhowalla, M. Evolution of Electrical , Chemical , and Structural Properties of Transparent and Conducting Chemically Derived Graphene Thin Films. *Adv. Funct. Mater.* **2009**, *8854*, 2577–2583.
- (13) De, S.; King, P. J.; Lotya, M.; Neill, A. O.; Doherty, E. M.; Hernandez, Y.; Duesberg, G. S.; Coleman, J. N. Flexible , Transparent , Conducting Films of Randomly Stacked Graphene from Surfactant-Stabilized , Oxide-Free Graphene Dispersions. *Small* **2010**, *6*, 458–464.
- (14) Li, X.; Cai, W.; An, J.; Kim, S.; Nah, J.; Yang, D.; Colombo, L.; Ruoff, R. S. Large-Area Synthesis of High-Quality and Uniform Graphene Films on Copper Foils. *Science* (80-.). **2009**, *3893*, 1312–1315.
- (15) Bae, S.; Kim, H.; Lee, Y.; Xu, X.; Park, J.-S.; Zheng, Y.; Balakrishnan, J.; Lei, T.; Ri

- Kim, H.; Song, Y. Il; *et al.* Roll-to-Roll Production of 30-Inch Graphene Films for Transparent Electrodes. *Nat. Nanotechnol.* **2010**, *5*, 574–578.
- (16) Reina, A.; Jia, X.; Ho, J.; Nezich, D.; Son, H.; Bulovic, V.; Dresselhaus, M. S.; Kong, J. Large Area , Few-Layer Graphene Films on Arbitrary Substrates by Chemical Vapor Deposition 2009. *Nano Lett.* **2009**, *9*, 30–35.
- (17) Li, X.; Magnuson, C. W.; Venugopal, A.; An, J.; Suk, J. W.; Han, B.; Borysiak, M.; Cai, W.; Velamakanni, A.; Zhu, Y.; *et al.* Graphene Films with Large Domain Size by a Two-Step Chemical Vapor Deposition Process. *Nano Lett.* **2010**, *10*, 4328–4334.
- (18) Novoselov, K. S.; Geim, A. K.; Morozov, S. V; Jiang, D.; Katsnelson, M. I.; Grigorieva, I. V; Dubonos, S. V; Firsov, A. A. Two-Dimensional Gas of Massless Dirac Fermions in Graphene. *Nature* **2005**, *438*, 197–200.
- (19) Neto, A. H. C.; Guinea, F.; Peres, N. M. R.; Novoselov, K. S.; Geim, A. K. The Electronic Properties of Graphene. *Rev. Mod. Phys.* **2009**, *81*, 109–162.
- (20) Sutter, P. W.; Flege, J.; Sutter, E. L. I. A. Epitaxial Graphene on Ruthenium. *Nat. Mater.* **2008**, *7*, 406–411.
- (21) Mattevi, C.; Chhowalla, M. A Review of Chemical Vapour Deposition of Graphene on Copper †. *J. Mater. Chem.* **2011**, *21*, 3324–3334.
- (22) Srivastava, A.; Galande, C.; Ci, L.; Song, L.; Rai, C.; Jariwala, D.; Kelly, K. F.; Ajayan, P. M. Novel Liquid Precursor-Based Facile Synthesis of Large-Area Continuous , Single , and Few-Layer Graphene Films. *Chem. Mater.* **2010**, *22*, 3457–3461.
- (23) Mittemeijer, E. J.; L, G. A. The Solubility of C in Solid Cu. **2004**, *51*, 1–5.
- (24) Hao, Y.; Bharathi, M. S.; Wang, L.; Liu, Y.; Chen, H.; Nie, S.; Wang, X.; Chou, H.; Tan, C.; Fallahzad, B.; *et al.* The Role of Surface Oxygen in the Growth of Large Single-Crystal Graphene on Copper. *Science (80-.)*. **2013**, *342*, 720–724.
- (25) Zhang, Z.; Du, J.; Zhang, D.; Sun, H.; Yin, L.; Ma, L.; Chen, J.; Ma, D.; Cheng, H.; Ren, W. Rosin-Enabled Ultraclean and Damaga-Free Transfer Graphene for Large-Area Flexible Organic Light-Emitting Diodes. *Nat. Commun.* **2017**, *8*, 1–9.
- (26) Kim, S. M.; Hsu, A.; Lee, Y.; Dresselhaus, M.; Kim, K. K.; Kong, J. The Effect of Copper Pre-Cleaning on Graphene Synthesis. *Nanotechnology* **2013**, *24*, 365602.
- (27) Jin, H.; Meyer, J.; Roth, S. Growth and Properties of Few-Layer Graphene Prepared by Chemical Vapor Deposition. *Carbon N. Y.* **2010**, *48*, 1088–1094.
- (28) Zhu, S. E.; Yuan, S.; Janssen, G. C. A. M. Optical Transmittance of Multilayer Graphene. *EPL* **2014**, *108*, 17007.
- (29) Goldberg, B. B.; Jorio, A.; Filho, A. G. S.; Dresselhaus, G.; Dresselhaus, M. S.; Swan, A. K. G -Band Resonant Raman Study of 62 Isolated Single-Wall Carbon Nanotubes. *Phys. Rev. B* **2002**, *65*, 155412.
- (30) Liu, Y.; Liu, Z.; Lew, W. S.; Wang, Q. J. Temperature Dependence of the Electrical Transport Properties in Few-Layer Graphene Interconnects. *Nanoscale Res. Lett.* **2013**, *8*, 335.
- (31) Jorio, A.; Dresselhaus, M. S.; Saito, R.; Dresselhaus, G. Raman Spectroscopy in Graphene Related System. *Weinheim: Wiley* **2011**.
- (32) Li, H.; Wu, J.; Huang, X.; Lu, G.; Yang, J.; Lu, X.; Xiong, Q.; Zhang, H. Rapid and Reliable Thickness Identifi Cation of Two-Dimensional Nanosheets Using Optical Microscopy. *ACS Nano* **2013**, *7*, 10344–10353.
- (33) Wang, L.; Williams, C. M.; Boutilier, M. S. H.; Kidambi, P. R.; Karnik, R. Single-Layer Graphene Membranes Withstand Ultrahigh Applied Pressure. *Nano Lett.* **2017**, *17*, 3081–

- 3088.
- (34) Chiu, P. Graphene Annealing : How Clean Can It Be ? *Nano Lett.* **2012**, *12*, 414–419.
 - (35) Han, Y.; Zhang, L.; Zhang, X.; Ruan, K.; Cui, L.; Wang, Y. Surface Transfer of Graphene Films via an Effective Sandwich Method for Organic Light- Emitting Diode Applications. *J. Mater. Chem. C* **2014**, *2*, 201–207.
 - (36) Wu, S. Surface Tension of Solids: An Equation of State Analysis 1. *J. Colloid Interface Sci.* **1979**, *71*, 1–5.
 - (37) Wu, S. Calculation of Interfacial Tension in Polymer Systems. *J. Polym. Sci. Part C* **1971**, *30*, 19–30.